© 2003 The Chemical Society of Japan Bull. Chem. Soc. Jpn., 76, 1093–1113 (2003)

Accounts

Structures and Magnetic Properties of Double Perovskites A_2LnMO_6 and 6H-Perovskites $Ba_3LnRu_2O_9$ (A = Sr, Ba; Ln = Y, Lanthanides; M = Nb, Ta, Ru)

Yukio Hinatsu* **and Yoshihiro Doi**

Division of Chemistry, Graduate School of Science, Hokkaido University, Sapporo 060-0810

(Received January 6, 2003)

This account describes the synthesis, crystal structures and magnetic properties of double perovskites A_2LnMO_6 and 6H-perovskites $Ba_3LnRu_2O_9$ (A = Sr, Ba; Ln = Y, lanthanides; M = Nb, Ta, Ru). The double perovskites A_2LnMO_6 have two kinds of cations, Ln and M, in the B site of the perovskite ABO_3. These cations adopt the alternative ordered arrangement. Measurements of the magnetic susceptibility, specific heat, and powder neutron diffraction showed that all of the A_2LnRuO_6 compounds exhibited an antiferromagnetic transition at low temperatures and a complex temperature dependence of the magnetic susceptibility below their transition temperatures. In these compounds, the magnetic interaction between the Ln (4f electrons) and Ru (4d electrons) ions via the Ln–O–Ru pathway contributes greatly to their magnetic cooperative phenomena. The structural and magnetic studies for the 6H-perovskites $Ba_3LnRu_2O_9$ show that the Ln cations occupy the corner-sharing octahedra (LnO_6 octahedron) and the Ru cations occupy the face-sharing octahedra (Ru_2O_9 dimer). The $Ba_3LnRu_2O_9$ compounds show a characteristic temperature-dependence of the magnetic susceptibilities, that is, a broad maximum at temperatures above 135 K and a magnetic transition at 5–15 K. These magnetic properties mainly reflect two kinds of the magnetic interactions: the interaction between Ln and Ru ions and that between Ru ions in the Ru_2O_9 dimer.

The perovskite-type oxide has the general formula ABO_3, in which A represents a large metal cation and B represents a small one. Figure 1 shows the typical structure of the cubic perovskite ABO_3. The perovskite structure can be described as a framework of corner-shared BO_6 octahedra. This structural feature is appropriate for the investigation of the magnetic interaction between the B site ions, because the perovskite has a linear alignment of B–O–B. Generally, the mechanism of the magnetic interaction between magnetic ions in a localized electron system is the superexchange interaction via an intermediate anion between them; such an interaction becomes strong when the angle of the superexchange pathway is 90° or 180°.[1] By reflecting the magnetic interaction via a 180° B–O–B pathway, the perovskite show various magnetic properties.[2]

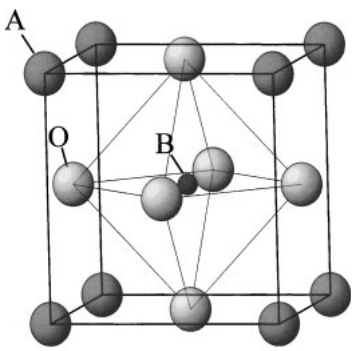

Fig. 1. The schematic structure of cubic ABO_3 perovskite.

These perovskite-type oxides have some flexibility in the chemical composition and the crystal structure; the combination of many kinds of ions and the control of their crystal structures are possible. Therefore, the perovskite-related compounds can show a variety of physical properties reflecting the nature of the constituent cations. Since the discovery of the high-temperature superconductivity in perovskite-related oxides containing copper,[3] many studies on the transition metal oxides have been performed to elucidate the mechanism of high-temperature superconductivity and to search for new superconductors. Besides the superconductivity, many interesting physical properties such as ionic conductivity,[4] ferroelectricity,[5] and giant magnetoresistance[6] have been found in the transition metal oxides with the perovskite-related structure.

Our concern is with the magnetic properties of the oxides containing lanthanide ions. The most stable oxidation state of lanthanide (Ln) ions is trivalent, and the electronic configuration of Ln^{3+} ions is $[Xe]4f^n$ ([Xe]: xenon electronic core). The magnetic properties of the lanthanide ions are fascinating for the reason of their systematic variety and intelligible complexity. Their magnetic properties are determined by

the unpaired 4f electrons. They are highly localized electrons, and the orbital contributions to their magnetic moments are significant. These features are in contrast with those of d electrons: the d orbitals are located in the valence shell and their contributions to the magnetic moments are essentially quenched. Generally, the shielding by the surrounding 5s and 5p electrons in the outer shell makes the magnetic interactions between 4f electrons in the condensed matter very weak, compared with those between d electrons. In fact, many of the lanthanide oxides order magnetically at < 4 K.[7]

One of the most challenging problems in the modern chemistry of lanthanide compounds is to find a compound in which strong magnetic superexchange interactions between 4f electrons exist, which give rise to a long-range magnetic ordering at relatively high temperatures, and to elucidate their mechanism. We have been focusing our attention on the crystal structures of the perovskite-type compounds containing lanthanide ions. The lanthanide ion is relatively large and tends to adopt a high coordination number. Therefore, the lanthanide ion usually sits at the A site of the perovskite-oxide ABO_3. As described already, the perovskites have some flexibility of chemical composition and the possibility of combination of many kinds of ions. By selecting large alkaline earth elements such as Sr and Ba as the A site atoms, one finds that lanthanides occupy the 6-coordinate B sites. Not the A site ions but the B site ions normally determine the physical properties of the perovskites ABO_3. In order to elucidate the behavior of 4f electrons which systematize the lanthanide series, we have investigated the crystal structures and magnetic properties of many ABO_3-type perovskites containing lanthanide ions at the B-site.[8–15] Among them, it is noteworthy that $BaPrO_3$, $SrTbO_3$, and $BaTbO_3$ show antiferromagnetic transitions at relatively high temperatures, i.e., 11.5, 32.0, and 33.4 K, respectively.[8,9,13]

Now, our interests are turned to the perovskite oxides containing both the lanthanide ions and transition metal ions (M) at the B sites. Solid state chemistry of perovskite-type oxides containing ruthenium has recently attracted a great deal of interest. These materials adopt a diverse range of structures and show a wide range of magnetic and electronic properties. For example, reports have featured the perovskite $SrRuO_3$ (metallic and ferromagnetic behavior below 160 K),[16] the layered perovskite Sr_2RuO_4 (superconductivity below 1 K),[17] the pyrochlores $Tl_2Ru_2O_7$ (metal-insulator transition at 125 K),[18] and $Ln_2Ru_2O_7$ (spin-glass like behavior below 80 K).[19]

In this account, we focus our attention on the perovskite-related oxides containing both lanthanide and ruthenium ions, such as double perovskites A_2LnRuO_6 and 6H-perovskites $A_3LnRu_2O_9$; we have studied their structural and magnetic properties. The contents of this paper are as follows. In section 1, we describe the crystal structure and magnetic properties of the double perovskites $A_2Ln^{3+}M^{5+}O_6$ (A = Sr, Ba; Ln = Y, lanthanides, M = Nb, Ta) in which only Ln ions are magnetic. Some basic knowledge about the A_2LnMO_6-type compounds is obtained, i.e., the crystal structure (distortion of the structure, order/disorder arrangement of the B site ions, and the chemical environment at the B site, etc.) and the magnetic behavior of the 4f electrons of the Ln^{3+} ions in the octahedral crystal field environment. In section 2, we discuss the magnetic properties of the double perovskites $A_2Ln^{3+}Ru^{5+}O_6$ compounds. They have shown antiferromagnetic transitions at low temperatures. Magnetic susceptibility, specific heat and neutron diffraction measurements have revealed that this magnetic transition is due to the antiferromagnetic ordering of both Ru^{5+} and Ln^{3+} ions. In section 3, we report the crystal structure and magnetic properties of 6H-perovskites $Ba_3LnRu_2O_9$. This crystal structure consists of the linkage of the LnO_6 octahedra and Ru_2O_9 dimers. They have shown a characteristic temperature-dependence of the magnetic susceptibilities. In these compounds, there exist magnetic interactions between 4f electrons of lanthanide ions, those between 4d electrons of ruthenium ions, and those between the 4f and 4d electrons. The principal motivation of this study is to investigate systematically the structural and magnetic properties of these compounds, and to elucidate each of the magnetic interactions.

1. Double Perovskites A_2LnMO_6 (A = Sr, Ba; Ln = Y, Lanthanides; M = Nb, Ta)

The double perovskites Ba_2LnTaO_6,[20,21] Ba_2LnNbO_6,[22] and Sr_2LnTaO_6[23] adopt the charge configuration $A^{2+}{}_2Ln^{3+}M^{5+}O_6$. In these compounds, only Ln^{3+} ions contribute to the magnetic behavior, because the Sr^{2+}, Ba^{2+}, Nb^{5+}, and Ta^{5+} ions are diamagnetic. Therefore, these compounds are appropriate for investigating the magnetic properties of 4f electrons in the B sites of the perovskites ABO_3. This section describes the structural and magnetic properties of Ba_2LnTaO_6, Ba_2LnNbO_6, and Sr_2LnTaO_6, by using the powder X-ray diffraction, magnetic susceptibility, ^{151}Eu Mössbauer spectroscopy, and electron paramagnetic resonance (EPR) measurements.

Synthesis and Crystal Structures of A_2LnNbO_6 and A_2LnTaO_6. Polycrystalline samples of Ba_2LnTaO_6, Ba_2LnNbO_6, and Sr_2LnTaO_6 were synthesized by the solid-state reaction method. Starting materials were $BaCO_3$, $SrCO_3$, Nb_2O_5, Ta_2O_5, Ln_2O_3 (Ln = Y, La, Nd, Sm–Gd, Dy–Lu), Pr_6O_{11}, and Tb_4O_7. These reagents were weighed in appropriate metal ratios and ground intimately in an agate mortar. The mixtures were pressed into pellets and the pellets were calcined at 1173 K. The calcined materials were reground and sintered in air at 1573–1773 K for several days with intermediate regrinding and repelletizing.

The results of the X-ray diffraction measurements show that these compounds have a single phase. Their X-ray diffraction patterns were indexed with a cubic unit cell (space group $Fm\bar{3}m$; $2a_p \times 2a_p \times 2a_p$) for some of A = Ba compounds or with a monoclinic unit cell (space group $P2_1/n$; $\sqrt{2}a_p \times \sqrt{2}a_p \times 2a_p$) for the others, where a_p represents a unit cell parameter of the primitive perovskite ($a_p \approx 4$ Å). The diffraction reflection at $2\theta \approx 18^\circ$ was found for each compound; this indicates that Ln and M ions in the A_2LnMO_6 order alternatively. These space groups all permit an NaCl-type ordered arrangement of the Ln and M ions.[24] The crystal structures of A_2LnMO_6 are illustrated in Fig. 2.

The difference in the crystal structure can be explained by the geometrical relationship between constituent ions. For double perovskites $A_2B'B''O_6$, the tolerance factor t is defined

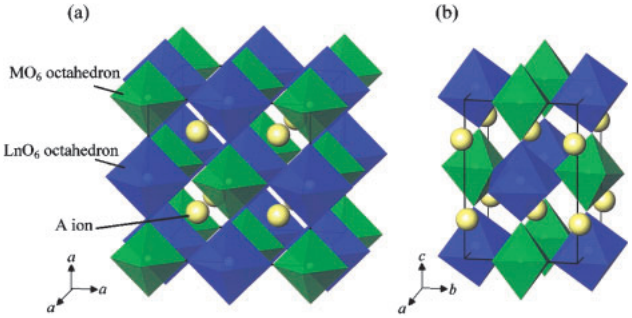

Fig. 2. Crystal structures of ordered perovskites A_2LnMO_6: (a) cubic and (b) monoclinic structures.

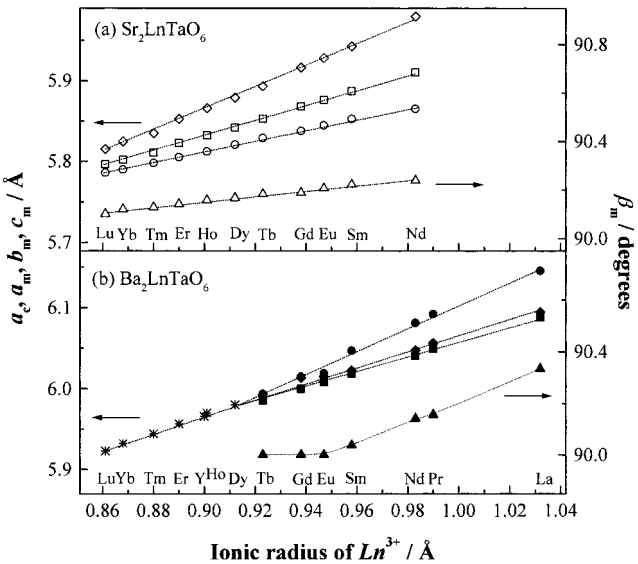

Fig. 3. Variation of lattice parameters for (a) Sr_2LnTaO_6 (○: a_m, ◇: b_m, □: $c_m/\sqrt{2}$, △: β_m) and (b) Ba_2LnTaO_6 (✻: a_c; ●: a_m, ◆: b_m, ■: $c_m/\sqrt{2}$, ▲: β_m).

by

$$t = \frac{r_A + r_O}{\sqrt{2}\left(\frac{r_{B'} + r_{B''}}{2} + r_O\right)}, \quad (1)$$

where r_A, $r_{B'}$, $r_{B''}$, and r_O are the ionic radii of the A, B′, B″, and O ions, respectively. For an ideal cubic perovskite structure, the value of t is equal to unity, whereas for structures distorted from the cubic symmetry, the value of t is usually <1. It is expected from Eq. 1 that the distortion of the crystal structure of A_2LnMO_6 will become more significant with decreasing the ionic size of the A ion and with increasing that of the Ln or M ion. Actually, a series of Ba_2LnTaO_6 compounds adopts structures more and more distorted from the cubic symmetry with increasing the ionic size of Ln ions, i.e., they have the cubic (for Ln = Y, Dy–Lu), or monoclinic (for Ln = La, Pr, Nd, Sm–Tb) structures.[20] All the Sr_2LnTaO_6 compounds are monoclinic, because the size of the Sr^{2+} ion at the A site is sufficiently smaller than that of the Ba^{2+} ion.[23]

Figure 3 shows the variation of lattice parameters for Sr_2LnTaO_6 and Ba_2LnTaO_6 with the ionic radius of Ln^{3+} in the six-coordination.[20,23] The lattice parameters, a_m, b_m, c_m (for the monoclinic cell), and a_c (for the cubic cell) increase

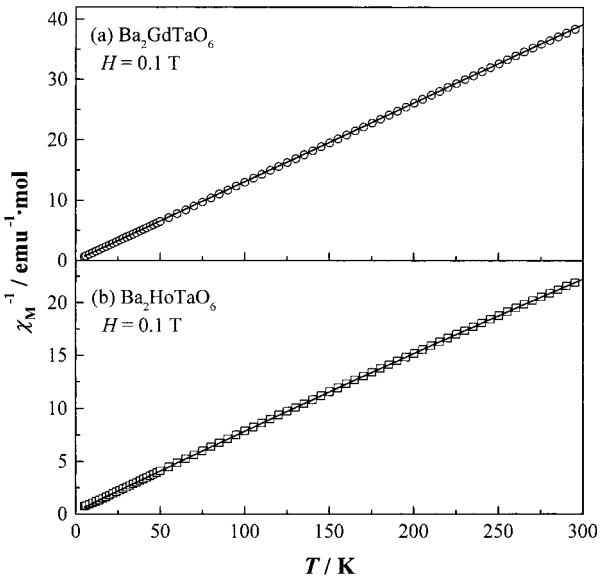

Fig. 4. Temperature dependence of the inverse magnetic susceptibilities of (a) Ba_2GdTaO_6 and (b) Ba_2HoTaO_6. Solid lines show the Curie–Weiss law fitting.

with the Ln^{3+} ionic radius. In the monoclinic region, the lattice parameter β_m increases and the differences among a_m, b_m and $c_m/\sqrt{2}$ spread with increase of the Ln^{3+} ionic radius. This fact indicates that the crystal structures of A_2LnTaO_6 are more distorted from the cubic symmetry as the size of Ln^{3+} ion becomes larger. This tendency has been also found in the crystal structures of other double perovskites A_2LnMO_6 (A = Sr, Ba; Ln = Y, lanthanide; M = Nb, Ru, Ir, Re).[22,25–28]

Magnetic Properties of A_2LnNbO_6 and A_2LnTaO_6. Since the Nb^{5+} and Ta^{5+} ions are diamagnetic, only the Ln^{3+} ions contribute to the magnetic behavior of A_2LnNbO_6 and A_2LnTaO_6. All the compounds are paramagnetic down to 5 K.[20–23] Figure 4 shows the temperature dependence of the inverse magnetic susceptibilities for Ba_2LnTaO_6 (Ln = Gd, Ho).[20] The susceptibilities were fitted with the Curie–Weiss law, and the effective magnetic moments and Weiss constants were obtained. The effective magnetic moments are consistent with the free-ion ones assuming that $\Delta E \gg k_B T$, where ΔE is the energy difference between the excited and ground states of the electronic multiplet, and k_B is the Boltzmann constant.

Figure 5 shows the temperature dependence of the inverse magnetic susceptibilities for Ba_2YbTaO_6. At lower temperatures, the temperature dependence of the susceptibility deviates from the Curie–Weiss relationship. This magnetic behavior has been found for some compounds and may be due to the crystal field splitting of the Ln^{3+} ions. In the Yb compound, the ground state $^2F_{7/2}$ of Yb^{3+} is split into two doublets (Γ_6 and Γ_7) and one quartet (Γ_8) in the octahedral symmetry (Fig. 6).[29] In this case, the magnetic susceptibility of Yb^{3+} ion is given by the following Van Vleck's equation:[30]

$$\chi_M(Yb^{3+}) = \frac{N_A g_J^2 \mu_B^2 J(J+1)}{3k_B T} \times \frac{98 + 260e^{-b} + 162e^{-a} + 432(e^{-b} - e^{-a})/(a-b) + 560(1 - e^{-b})/b}{378\,(1 + 2e^{-b} + e^{-a})}, \quad (2)$$

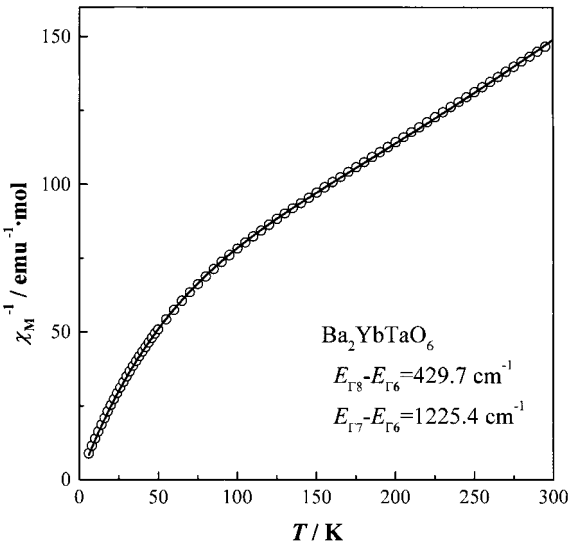

Fig. 5. Temperature dependence of the inverse magnetic susceptibilities of Ba_2YbTaO_6. A solid line shows the calculation result by Eq. 2.

where N_A, g_J, and μ_B are the Avogadro number, Landé g factor, and Bohr magneton, respectively, and $a = (E_{\Gamma 7} - E_{\Gamma 6})/k_B T$ and $b = (E_{\Gamma 8} - E_{\Gamma 6})/k_B T$. By fitting Eq. 2 to the experimental magnetic susceptibilities (Fig. 5), we determined the energy difference between the Γ_6 ground state and the Γ_7 or Γ_8 excited state to be $E_{\Gamma 8} - E_{\Gamma 6} = 368$–$430$ cm^{-1} and $E_{\Gamma 7} - E_{\Gamma 6} = 1058$–$1324$ cm^{-1} for Ba_2YbTaO_6, Ba_2YbNbO_6, and Sr_2YbTaO_6.[21–23]

For Ln = Sm and Eu compounds, the temperature dependences of magnetic susceptibilities do not obey the Curie–Weiss law. This is due to the contribution from the excited multiplet of Ln^{3+} ions to the magnetic susceptibility. The ground states of the Sm^{3+} and Eu^{3+} are $^6H_{5/2}$ and $^7F_0$, respectively. However, the energy difference between the ground state and the excited state $^6H_{7/2}$ for Sm^{3+} or ^7F_J ($J = 1, 2, \ldots, 6$) for Eu^{3+} is not so large compared with $k_B T$. Hence, the population to the excited state must be taken into consideration in the calculation of magnetic susceptibility at higher temperatures. For the case of the Eu^{3+} ion, the molar magnetic susceptibility can be expressed by the following equation:[30]

$$\chi(\mathrm{Eu}^{3+}) = \frac{N_A \mu_B^2}{3 k_B \gamma T} \times \frac{24 + (13.5\gamma - 1.5)e^{-\gamma} + (67.5\gamma - 2.5)e^{-3\gamma} + (189\gamma - 3.5)e^{-6\gamma}}{1 + 3e^{-\gamma} + 5e^{-3\gamma} + 7e^{-6\gamma}}, \quad (3)$$

where $\gamma = \lambda/k_B T$ is 1/21 of the ratio of the overall multiplet width to $k_B T$, and λ is the spin-orbit coupling constant. When the calculated magnetic susceptibility was fitted to the experimental susceptibilities, the spin-orbit coupling constants for Sm^{3+} and Eu^{3+} were determined to be 287–317 cm^{-1} and 331–339 cm^{-1}, respectively.[20,22,23]

The ^{151}Eu Mössbauer spectroscopy and electron paramagnetic resonance (EPR) measurements have been carried out. Figure 7 shows the ^{151}Eu Mössbauer spectrum for Ba_2EuTaO_6 at room temperature.[20] The isomer shifts of A_2EuMO_6 compounds are 1.4–1.5 mm s^{-1}, which confirms that the europium ions are in the trivalent state.[31] The peak shape of the spectra

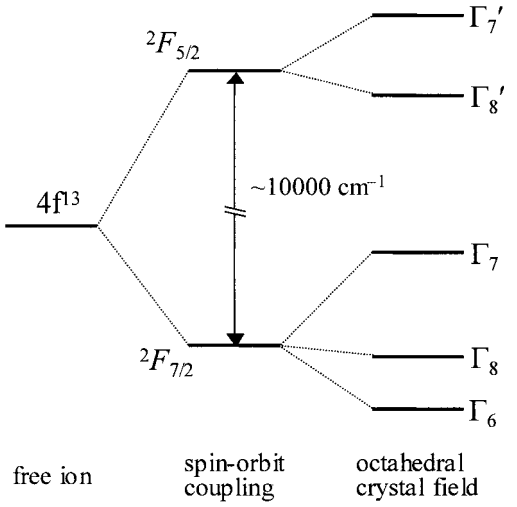

Fig. 6. The energy level diagram for the configuration 4f^{13} in an octahedral crystal field.

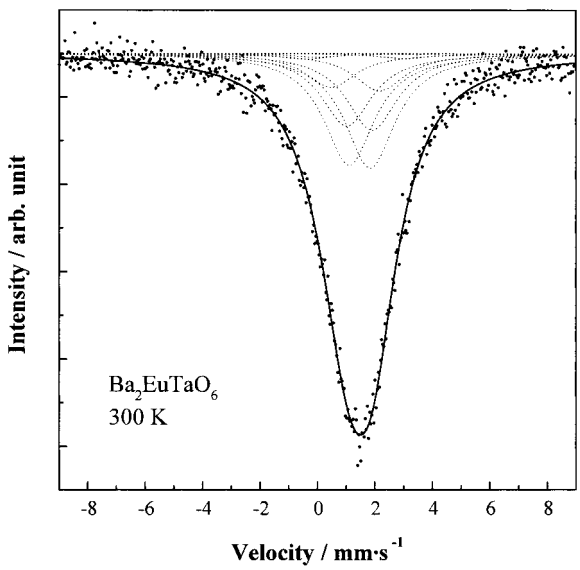

Fig. 7. ^{151}Eu Mössbauer spectrum of Ba_2EuTaO_6 at 300 K.

is not symmetrical, which indicates the existence of an electric field gradient tensor at the Eu site due to the low symmetry of this site. Taking into account this asymmetry and the quadrupole interaction of ^{151}Eu nuclei, one can explain the observed data by the sum of peaks from the 12 possible transitions (Fig. 8).

Figure 9 shows the EPR spectrum measured at 8 K of a crystal where Yb^{3+} ions are doped in the Ba_2LuTaO_6.[21] The hyperfine interaction has been observed for the EPR spectrum. For ytterbium, there are seven isotopes. Among them, ^{171}Yb (natural abundance 14.3%) and ^{173}Yb (natural abundance 16.1%) have nuclear spins of $I = 1/2$ and 5/2, respectively. In this Yb^{3+}/Ba_2LnTaO_6 crystal, the spacings between EPR absorption lines become wider with resonance magnetic field, which indicates that the electron spin quantum number and the nuclear spin quantum number are not good quantum numbers. The results of fitting the spin Hamiltonian to the observed EPR spectrum are also shown in Fig. 9 by depicting the isotopic

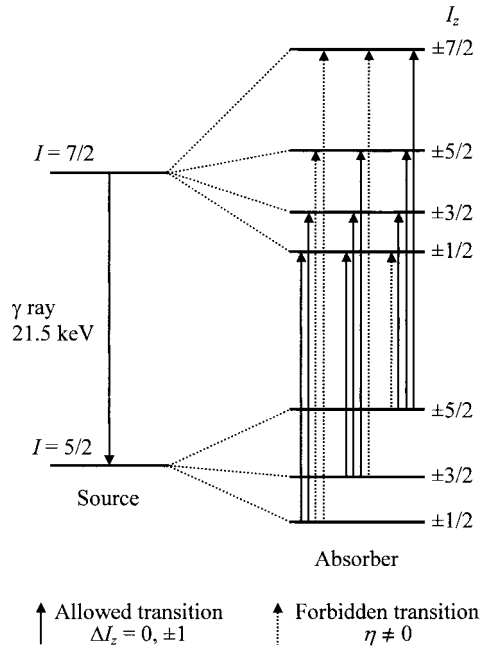

Fig. 8. Twelve possible transitions by the quadrupole interaction of ^{151}Eu nuclei.

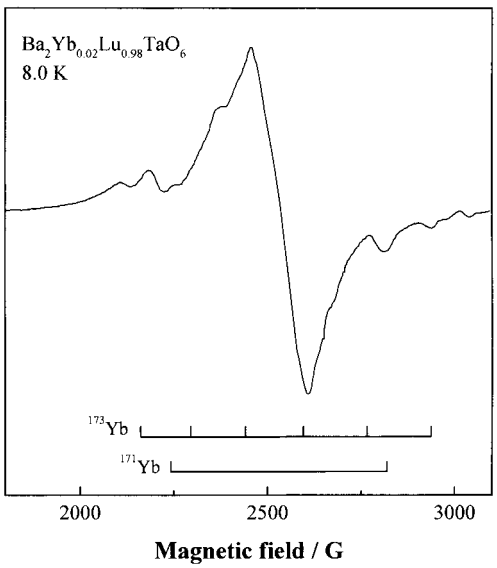

Fig. 9. EPR spectrum of an Yb^{3+} ion doped in Ba_2LuTaO_6 measured at 8 K. Isotropic EPR absorption lines for $I = 1/2$ and $I = 5/2$ are depicted with the stick diagram below.

EPR absorption lines with the stick diagram. The g values and hyperfine coupling constants were determined by the analysis of this spectrum.[21] They show the existence of covalent bonding in the Yb^{3+} ion, i.e., the covalent contribution of the s and p orbitals from the O^{2-} ion to the empty 4f orbital of the Yb^{3+} ion.[32,33]

Summary of Double Perovskites A_2LnNbO_6 and A_2LnTaO_6. The double perovskites Ba_2LnTaO_6, Ba_2LnNbO_6, and Sr_2LnTaO_6 have an ordered perovskite structure, in which the two B-site ions, Ln and Ta/Nb, are ordered alternatively. These compounds are paramagnetic down to 5 K, and no evidence for the magnetic ordering of Ln^{3+} ions has been observed. This result is quite contrastive to the results for some $ALnO_3$ perovskites (A = Sr, Ba, La, Ce, Pr; Ln = paramagnetic lanthanide ions). Most of them show a magnetic transition at low temperatures.[8,9,11–13,15] For example, $SrTbO_3$ and $BaTbO_3$ both show an antiferromagnetic transition by the magnetic ordering of Tb^{4+} ions at 32.0 and 33.4 K, respectively.[13] In the double perovskites A_2LnMO_6 (M = Nb, Ta), half of the B-site ions are occupied with nonmagnetic M^{5+} ions, which makes the magnetic interaction between Ln^{3+} ions very weak.

2. Double Perovskites A_2LnRuO_6 (A = Sr, Ba; Ln = Y, Lanthanides)

This section describes the crystal structures and magnetic properties of the double perovskites A_2LnRuO_6 (A = Sr, Ba; Ln = Y, lanthanides). These compounds have pentavalent ruthenium ions at the B sites; two kinds of B site ions, Ln^{3+} and Ru^{5+}, order alternatively. The perovskite-related oxides containing ruthenium ions often exhibit interesting magnetic and electronic properties.[16,17] Therefore, the A_2LnRuO_6 compounds should also show various attractive magnetic properties. In addition, since they contain both ruthenium and lanthanide ions, we may observe magnetic cooperative phenomena due to the interactions between d electrons (ruthenium) and 4f electrons (lanthanides).

Crystal Structures and Magnetic Properties of Sr_2LnRuO_6. Polycrystalline samples of Sr_2LnRuO_6 (Ln = Eu–Lu) were synthesized by firing the mixtures of strontium carbonate, lanthanide oxides, and ruthenium dioxide (RuO_2), initially at 1173 K in air for 12 h and then at 1473–1573 K for several days with several intermediate grindings and pelletings. Their X-ray diffraction patterns were indexed on a monoclinic unit cell (space group $P2_1/n$). Their structural analyses using the Rietveld method show that the Ln and Ru ions are arranged in an alternating manner (NaCl-type).

The Sr_2LnRuO_6 compounds show a variety of temperature dependences of magnetic susceptibilities at low temperatures.[25] The susceptibility measurements show that the antiferromagnetic transition occurs in all the Sr_2LnRuO_6 compounds. Figure 10 shows the temperature dependence of the magnetic susceptibilities for Sr_2HoRuO_6 and Sr_2TmRuO_6. Their Néel temperatures, effective magnetic moments and Weiss constants are listed in Table 1. In these magnetic transitions, the magnetic interaction between Ru^{5+} ions should operate significantly, because the transition temperatures do not exhibit such large differences among compounds. Generally, the antiferromagnetic ordering of Ru^{5+} ions in the Sr_2BRuO_6 (where B is a trivalent diamagnetic ion) is due to the superexchange interaction between nearest neighboring Ru^{5+} ions, i.e., the pathway is Ru–O–O–Ru or Ru–O–B–O–Ru.[38] In the present Sr_2LnRuO_6, two kinds of magnetic ions exist; therefore, not only the magnetic interaction between Ru^{5+} ions but also the interaction between Ln^{3+} and Ru^{5+} ions (the pathway is Ln–O–Ru) should contribute to the magnetic properties of these compounds. Since the interactions between Ln^{3+} ions are very weak, as is mentioned for Ba_2LnMO_6 (M = nonmagnetic Nb^{5+} and Ta^{5+} ions) in section 1, we need not con-

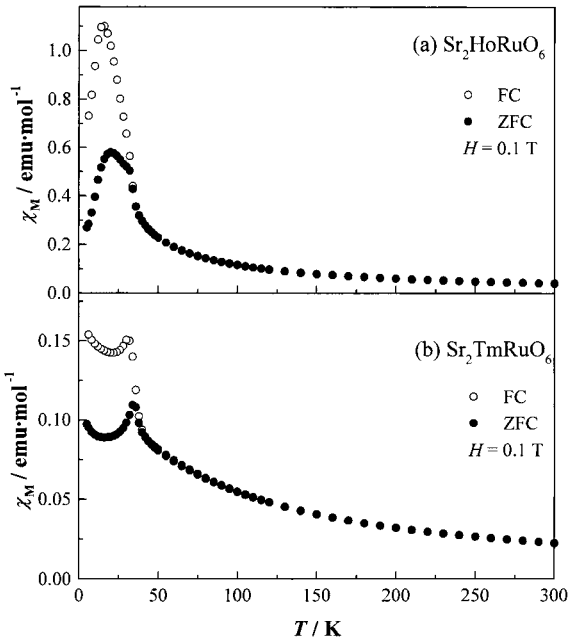

Fig. 10. Temperature dependence of the magnetic susceptibilities of (a) Sr_2HoRuO_6 and (b) Sr_2TmRuO_6.

Table 1. Néel Temperatures, Effective Magnetic Moments, and Weiss Constants for Sr_2LnRuO_6

Ln	T_N/K	μ_{eff}/μ_B	θ/K	Ref.
Y	26	3.13	−142	(34), (35)
Gd	31	7.1(2)	−8(1)	(25)
Tb	41	9.1(1)	−15(3)	(25)
Dy	38	10.4(2)	−20(3)	(25)
Ho	36	10.6(2)	−20(3)	(25)
Er	42	9.8(1)	−22(3)	(25)
		9.72(7)	−12(1)	(36)
Tm	36	8.1(1)	−47(4)	(25)
Yb	44	6.6(3)	−225(23)	(25)
Lu	30	3.2(1)	−205(15)	(25), (37)

sider their contributions to the magnetic ordering found in these Sr_2LnRuO_6 compounds.

For all the Sr_2LnRuO_6 compounds, the field dependence of the magnetization was measured at 10 K over the magnetic field range of $-5\ \mathrm{T} < H < 5\ \mathrm{T}$. Figure 11 shows the variation of magnetization as a function of magnetic field for Sr_2HoRuO_6 ($T_N = 36$ K) at various temperatures.[25] For all the compounds, small magnetic hysteresis was observed below the Néel temperature. In addition to this, a large divergence between the FC (field cooling condition) and ZFC (zero field cooling condition) susceptibilities was found. These experimental results indicate that Sr_2LnRuO_6 are not ideal antiferromagnets. This is probably due to the contribution of the weak ferromagnetic component to the magnetic property. In the case of the compounds with a low crystal symmetry such as monoclinic symmetry, the Dzyaloshinsky–Moriya (D–M) interaction can exist between the ordered elements, which results in the existence of a weak ferromagnetic component in their susceptibilities.[39]

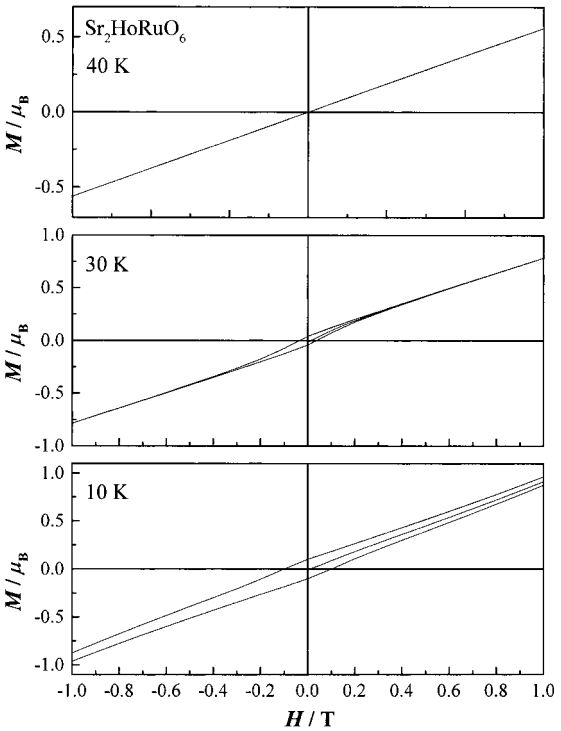

Fig. 11. Field dependence of the magnetization of Sr_2HoRuO_6 at 40, 30, and 10 K.

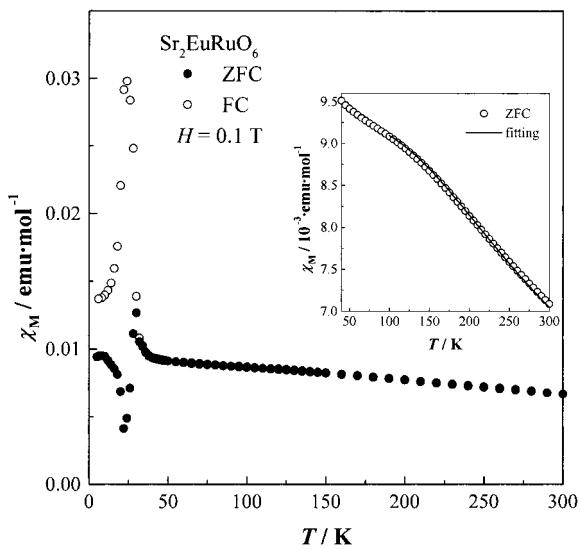

Fig. 12. Temperature dependence of the magnetic susceptibilities of Sr_2EuRuO_6. A solid line in the inset shows the calculation result by Eq. 4.

Figure 12 shows the temperature dependence of the magnetic susceptibility for Sr_2EuRuO_6;[25] it does not obey the Curie–Weiss law. This can be explained by the same reason as that for the A_2EuMO_6 (A = Sr, Ba; M = Nb, Ta) in section 1, i.e., the ground state $^7F_0$ of Eu^{3+} and the excited states ^7F_J ($J = 1, 2, \ldots, 6$) are close enough to give energy differences comparable to k_BT at room temperature. If the magnetic behavior of Eu^{3+} and Ru^{5+} ions is independent in the paramagnetic region, the susceptibility of Sr_2EuRuO_6 will be given by

the sum of the susceptibilities of each paramagnetic ion. In that case, the total magnetic susceptibility of Sr_2EuRuO_6 is given by

$$\chi_M = \chi(Eu^{3+}) + \chi(Ru^{5+}) + \chi_{TIP}, \quad (4)$$

where

$$\chi(Ru^{5+}) = \frac{N_A \mu_{eff}^2 \mu_B^2}{3k_B(T-\theta)},$$

and χ_{TIP} is the temperature-independent susceptibility of Sr_2EuRuO_6. By fitting Eq. 4 to the experimental susceptibility, one can estimate the effective magnetic moment and Weiss constant to be $\mu_{eff} = 3.1(1)\ \mu_B$ and $\theta = -399(16)$ K, respectively. The large negative Weiss constant indicates the existence of an antiferromagnetic interaction between Ru^{5+} ions.

The Néel temperatures for the Sr_2LnRuO_6 (Ln = Tb–Tm) compounds are higher than that for Sr_2LuRuO_6 ($T_N = 30$ K, Lu^{3+} is diamagnetic).[25,37] This fact indicates that the magnetic interactions between Ru^{5+} and Ln^{3+} ions greatly contribute to the antiferromagnetic ordering in the Sr_2LnRuO_6 compounds. The Néel temperature for Sr_2EuRuO_6 is close to that for Sr_2LuRuO_6. Since the ground state of Eu^{3+} ion, i.e., $^7F_0$ is nonmagnetic, the magnetic interaction between Eu^{3+} and Ru^{5+} ions is negligible for this antiferromagnetic transition.

Crystal Structures and Magnetic Properties of Ba_2LnRuO_6. Polycrystalline samples of Ba_2LnRuO_6 (Ln = Y, Pr, Nd, Er–Yb) were synthesized by firing the mixtures of barium carbonate, lanthanide oxides, and ruthenium dioxide, initially at 1173 K in air for 12 h and then at 1473–1573 K for several days, with several intermediate grindings and pelletings. The Rietveld analyses of their X-ray diffraction patterns show that the compounds with larger lanthanides (Ln = Pr and Nd) adopt a monoclinic unit cell (space group $P2_1/n$),[40,41] and that those with smaller lanthanides (Ln = Y, Er–Yb) adopt a cubic unit cell (space group $Fm\bar{3}m$).[42,43]

All the Ba_2LnRuO_6 compounds show an antiferromagnetic transition at lower temperatures and have higher Néel temperatures ($T_N = 30$–117 K) than those for the corresponding Sr_2LnRuO_6 compounds ($T_N = 26$–44 K). The magnetic transition temperatures and some magnetic parameters for Ba_2LnRuO_6 are listed in Table 2. We will describe in detail the magnetic properties of Ba_2YRuO_6 and Ba_2ErRuO_6 in the following.

Table 2. Néel Temperatures, Effective Magnetic Moments, and Weiss Constants for Ba_2LnRuO_6

Ln	T_N/K	μ_{eff}/μ_B	θ/K	Ref.
Y	37	4.5(2)	−630(9)	(37), (42)
La	29.5	4.00	−304	(35)
Pr	117	5.24(1)	−133(2)	(40)
Nd	57	4.96(1)	−35(1)	(41)
Gd	48	8.0	−13	(44)
Ho	51	10.8	−20	(45)
Er	40	9.52(2)	−14.6(5)	(42)
Tm	42	7.92(2)	−34(1)	(43)
Yb	48	4.20(6)	−181(6)	(43)
Lu	35	4.4(1)	−630(9)	(37)

The temperature dependence of the magnetic susceptibilities for Ba_2YRuO_6 is plotted in Fig. 13(a); it indicates the existence of a magnetic anomaly at 37 K. Figure 13(b) shows the variation of its specific heat as a function of temperature. The λ-type anomaly has been observed, which corresponds to the magnetic anomaly found in the magnetic susceptibility. This anomaly is due to the antiferromagnetic ordering of Ru^{5+} ions,[37,42] because Y^{3+} ions are diamagnetic.

Figure 14 shows the temperature dependence of the magnetic susceptibility and specific heat for Ba_2ErRuO_6. Two magnetic anomalies have been found at 10 and 40 K. We consider that the magnetic anomaly at 40 K is ascribable to the antiferromagnetic ordering of Ru^{5+} ions, and that the anomaly at 10 K is due to the magnetic interaction between Er^{3+} ions. Specific heat and neutron diffraction measurements have given the same results,[42] which will be described later. The reason why the magnetic transition at 40 K is not clear in the magnetic susceptibility vs temperature curve is due to the magnetic moment of the Ru^{5+} ion (3.87 μ_B) being smaller than that of the Er^{3+} ion (9.59 μ_B). Fitting of the Curie–Weiss law to the magnetic susceptibility gives the effective magnetic moment and Weiss constant to be 9.52(2) μ_B and −14.6(5) K, respectively. The value of the effective magnetic moment for Ba_2ErRuO_6 is lower than that calculated from the magnetic moments for the free ions of Ru^{5+} and Er^{3+} (10.3 μ_B). This result suggests that the magnetic ions in this compound are affected by the crystal field to some extent. The negative Weiss constant indicates that the predominant magnetic interaction in Ba_2ErRuO_6 is antiferromagnetic.

The specific heat data for diamagnetic compounds Ba_2YNbO_6 and Ba_2LuNbO_6 are also plotted in Figs. 13(b) and 14(b), respectively. These compounds are isomorphous with Ba_2YRuO_6 and Ba_2ErRuO_6. Generally, the specific heat

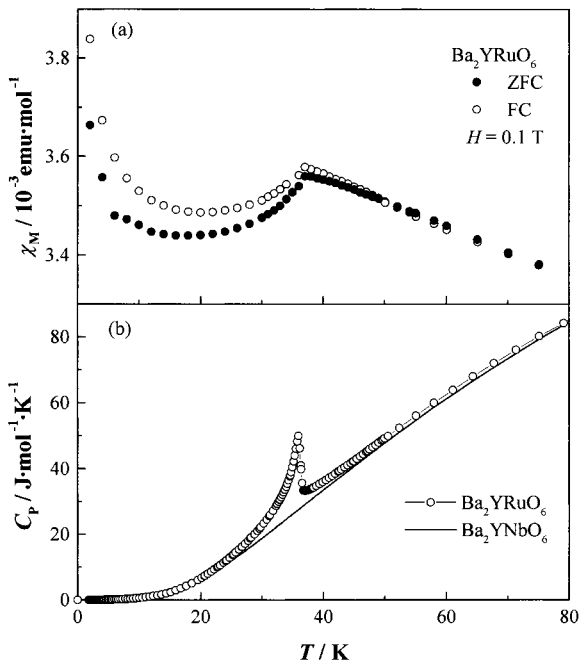

Fig. 13. Temperature dependence of (a) the magnetic susceptibilities and (b) specific heat of Ba_2YRuO_6. A solid line shows the specific heat of Ba_2YNbO_6.

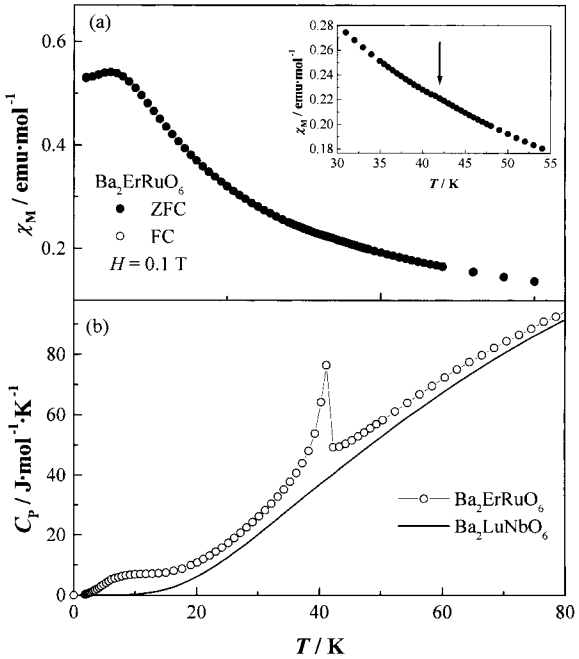

Fig. 14. Temperature dependence of (a) the magnetic susceptibilities and (b) specific heat of Ba_2ErRuO_6. A solid line shows the specific heat of Ba_2LuNbO_6. An arrow in the inset shows the magnetic transition temperature (see text).

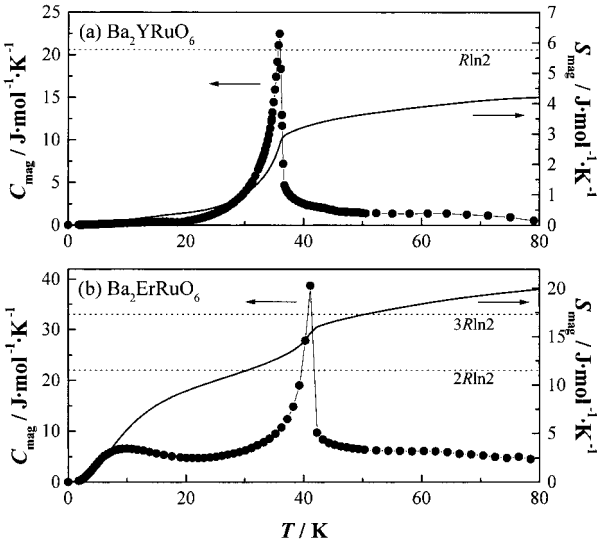

Fig. 15. Temperature dependence of the magnetic specific heat (C_{mag}) and magnetic entropy (S_{mag}) for (a) Ba_2YRuO_6 and (b) Ba_2ErRuO_6.

consists of the magnetic (C_{mag}), electronic (C_{elec}), and lattice contributions (C_{lat}). If we assume that the electronic and lattice contributions to the specific heat are equal between Ba_2YRuO_6 and Ba_2YNbO_6, the magnetic specific heat (C_{mag}) for Ba_2YRuO_6 is obtained by subtracting the specific heat of Ba_2YNbO_6 from that of Ba_2YRuO_6, because Ba_2YNbO_6 has no magnetic ions. This magnetic specific heat is due to the magnetic ordering of the Ru^{5+} ions in the Ba_2YRuO_6. The same procedures can be applied to the case for Ba_2ErRuO_6 and Ba_2LuNbO_6. By subtracting the specific heat of Ba_2LuNbO_6 from that of Ba_2ErRuO_6, the magnetic specific heat for Ba_2ErRuO_6 is obtained. In this case, the obtained magnetic specific heat is due to both the magnetic orderings of Ru^{5+} and Er^{3+} ions in the Ba_2ErRuO_6. The temperature dependence of the magnetic specific heat and the magnetic entropy ($S_{mag} = \int (C_{mag}/T)\,dT$) for Ba_2YRuO_6 and Ba_2ErRuO_6 is shown in Fig. 15. The magnetic entropy changes associated with the antiferromagnetic transition are obtained to be $\sim$3.9 J mol^{-1} K^{-1} for Ba_2YRuO_6 and $\sim$18 J mol^{-1} K^{-1} for Ba_2ErRuO_6. These magnetic entropy changes are near to $R\ln 2 = 5.76$ J mol^{-1} K^{-1} and $3R\ln 2 = 17.3$ J mol^{-1} K^{-1}, respectively (R: molar gas constant). The result for the Ba_2YRuO_6 means that the ground state of the Ru^{5+} ion should be doublet. That is, although a total spin quantum number of the Ru^{5+} is calculated to be $S = 3/2$, the four degenerating states split into two doublets $|S = 3/2, M_S = \pm 3/2>$ and $|S = 3/2, M_S = \pm 1/2>$.[46] If we presume that the same estimation for the magnetic entropy change of Ru^{5+} ions holds for the case of Ba_2ErRuO_6, the rest of the magnetic entropy due to the magnetic ordering of Er^{3+} ions is $3R\ln 2 - R\ln 2 = 2R\ln 2 = R\ln 4$. This result indicates that the degeneracy W (cf. $S = R\ln W$) of the ground state of Er^{3+} ion should be four. In the octahedral crystal field, the ground multiplet $^4I_{15/2}$ of the Er^{3+} splits and a Γ_7 doublet or a Γ_8 quartet becomes a ground state.[29] The results of the specific heat measurements indicate that the ground state of the Er^{3+} ion should be the Γ_8 quartet.

Magnetic Structures of A_2LnRuO_6. In order to determine the magnetic structures of A_2LnRuO_6, we performed the powder neutron diffraction measurements for many compounds. As an example, the neutron diffraction profiles for Sr_2TbRuO_6 at room temperature and 10 K are plotted in Fig. 16. The data collected at 10 K show a number of low angle peaks; these were not observed at room temperature, indicating that these compounds exhibit a long-range magnetic ordering at low temperatures. Neither superlattice reflections nor magnetic satellite reflections exist. The observed magnetic peaks can be indexed with the condition that [h + k + l] is an odd integer. Large (100) and (010) peaks are observed, while the (001) magnetic reflection is very weak, but has a detectable intensity; this fact indicates that the directions of the magnetic moments of Ln^{3+} and Ru^{5+} ions cant from the c axis to some extent. The Rietveld analysis of the neutron diffraction data measured at 10 K was performed. The magnetic structure determined for Sr_2HoRuO_6 is illustrated in Fig. 17(a). In this magnetic structure, both the magnetic moments of Tb^{3+} and Ru^{5+} ions are ordered antiferromagnetically. Each of the magnetic moments of Tb^{3+} and Ru^{5+} ions orders in a type I arrangement.[47]

The data concerning the magnetic structures of a series of A_2LnRuO_6 (A = Sr, Ba; Ln = Y, lanthanides) compounds are summarized in Table 3. The A_2LnRuO_6 (Ln = Ho, Er, Tm) compounds adopt the same magnetic structure as that of Sr_2TbRuO_6, while the A_2LnRuO_6 compounds with Ln = Pr, Nd, Yb adopt a magnetic structure that is different from the structure of Sr_2TbRuO_6. The difference between these magnetic structures is in the arrangement of the magnetic moments of Ln^{3+} and Ru^{5+} ions in the *ab* plane. For example, in the

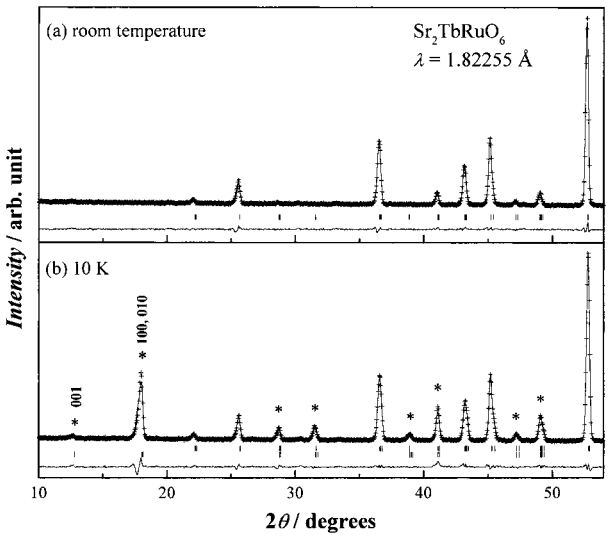

Fig. 16. Powder neutron diffraction profiles of Sr_2TbRuO_6 (a) at room temperature and (b) at 10 K. Marked (∗) peaks indicate the magnetic reflections.

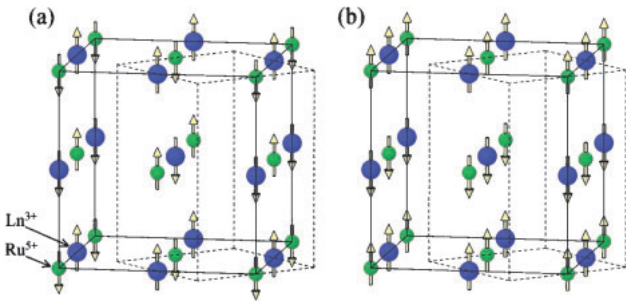

Fig. 17. Schematic magnetic structures of A_2LnRuO_6. Solid and dashed lines indicate the cubic and monoclinic unit cells, respectively.

case of Sr_2TbRuO_6, the moments of Ln^{3+} and Ru^{5+} are antiparallel with each other, while they are parallel for Ba_2PrRuO_6 (see Figs. 17(a) and (b)).

The ordered magnetic moments of Ru^{5+} are determined to be 1.5–3.0 μ_B. The theoretical value of the magnetic moment of Ru^{5+} ($4d^3$) is 3.0 μ_B. The difference in the ordered moments may be attributed to the thermal fluctuations of the magnetic moments[36] and/or the covalent effects. The ordered magnetic moments of Ln^{3+} are also smaller than the values expected from the free ion ($g_J J$). This can be explained by the same reasons (thermal fluctuation and covalent effect) and by the effect of the crystal field. For some Ln^{3+} ions, the latter effect is important. For example, the ordered magnetic moment of the free Yb^{3+} ion should be $g_J J = 4$ μ_B; however, the values determined by the analysis of the neutron diffraction data for Sr_2YbRuO_6 and Ba_2YbRuO_6 are only ~1 μ_B. The ground state of Yb^{3+} in the octahedral crystal field is the Γ_6 state.[29] The theoretical magnetic moment calculated from the Γ_6 state of Yb^{3+} is $g_J\langle\Gamma_6|J_z|\Gamma_6\rangle = 8/7 \times 7/6 = 1.33$ μ_B. This value is comparable with the ordered magnetic moments determined from the Rietveld analysis for the neutron diffraction data.

Table 3. Magnetic Structures of Ordered Perovskites A_2LnRuO_6 (A = Sr, Ba; Ln = Y, Lanthanides) Determined by Neutron Diffraction Measurements

Ln	A	Type of the ordering		Angle	Ordered moments /μ_B		T_m/K*3	Ref.
		Ru	Ln*1	/deg*2	Ru	Ln		
La	Ba	IIIa	—	(⊥*a*)	1.96(10)	—	2	(38)
Pr	Ba	I	I_p	0	2.0(2)	2.2(1)	7	(40)
Nd	Ba	I	I_p	90	2.2(1)	2.3(1)	7	(41)
Tb	Sr	I	I_a	~20	2.99(11)	4.98(12)	10	(47)
Ho	Sr	I	I_a	0	2.74(9)	6.66(8)	10	(48)
	Ba	I	I_a	0	2.9	9.7	10	(45)
Er	Sr	I	I_a	90	1.74(6)	4.59(3)	4.2	(36)
	Ba	I	I_a	90	2.87(13)	4.43(8)	10	(42)
Tm	Sr	I	I_a	0	1.5(1)	1.4(1)	10	(43)
	Ba	I	I_a	0	2.13(5)	1.91(3)	10	(43)
Yb	Sr	I	I_p	23(2)	3.0(2)	0.92(8)	10	(43)
	Ba	I	I_p	0	2.57(6)	1.00(3)	10	(43)
Lu	Sr	I	—	—*4	2.10(8)	—	4.2	(37)
	Ba	I	—	—*4	2.06(6)	—	4.2	(37)
Y	Sr	I	—	—*4	1.85(10)	—	4.2	(34)
	Ba	I	—	—*4	2.11(6)	—	4.2	(37)

Note: ∗1 I_p: parallel arrangement of magnetic moments between Ln and Ru ions in the *ab* plane, I_a: antiparallel arrangement; ∗2 direction of ordered magnetic moments against the *c* axis; ∗3 temperature for measurements, ∗4 at least $\neq 0°$ because a large (001) reflection was observed.

The magnetic structures of the A_2LnRuO_6 series are based on the type I ordering of Ru^{5+} and Ln^{3+} ions (see Fig. 17 and Table 3), except for the type IIIa ordering in Ba_2LaRuO_6. For Ln = Y, La, Lu compounds, only the Ru^{5+} ions are magnetic. For such cases, the type of the magnetic ordering of Ru^{5+} ions is determined by the relative strength of the two dominant magnetic interactions: one of these is the interactions between the nearest neighbor Ru^{5+} ions through the Ru–O–O–Ru pathway and the other one is the interactions between the next-nearest neighbor Ru^{5+} ions through the Ru–O–Ln–O–Ru pathway.[38] In the case that the Ln^{3+} ions are magnetic, their Néel temperatures are higher than those for the compounds containing the nonmagnetic Ln^{3+} ions, and the long range magnetic ordering of the Ln^{3+} ions has been also observed in the neutron diffraction measurements. These results indicate that both the magnetic interactions between Ru ions (Ru–O–O–Ru pathway) and the interactions between Ru and Ln ions (Ru–O–Ln pathway) contribute to the magnetic ordering of the Ru^{5+} and Ln^{3+} ions in the A_2LnRuO_6 compounds. For the Ba_2LnRuO_6 and Sr_2LnRuO_6 that include the same Ln ion, their magnetic structures are almost the same (see Table 3). The difference in the magnetic structures between the A_2LnRuO_6 compounds with the different Ln^{3+} ions should reflect the characteristics of each of the Ln^{3+} ($4f^n$) ions in the magnetic interactions between Ru and Ln ions.

Summary of Double Perovskites A_2LnRuO_6. The double perovskites A_2LnRuO_6 have an ordered perovskite structure in which the Ln and Ru ions are ordered alternatively. All the

A_2LnRuO_6 compounds show an antiferromagnetic transition at 30–117 K; this transition is due to the magnetic cooperative phenomena between Ru^{5+} ($4d^3$) and Ln^{3+} ($4f^n$) ions. If the number of 4f electrons is changed, they show a variety of magnetic properties at low temperatures. The neutron diffraction measurements show that the magnetic structures of these A_2LnRuO_6 compounds are based on the type I ordering of Ru^{5+} and Ln^{3+} ions.

3. 6H-Perovskites $Ba_3LnRu_2O_9$ (Ln = Y, Lanthanides)

This section describes the crystal structures and magnetic properties of perovskite-related compounds $Ba_3LnRu_2O_9$ (Ln = Y, lanthanides). They contain both the Ln and Ru ions as the B site ions of the perovskite ABO_3, in the ratio of 1:2. The increase in the proportion of smaller Ru ions makes the tolerance factor t (Eq. 1) large. As a result, the tolerance factor becomes ~1 or exceeds 1. In that case, such compounds often adopt a hexagonal perovskite structure; the 6H-$BaTiO_3$ type structure[49] is most likely.

Figure 18 shows the 6H-$BaTiO_3$ type structure; this has two kinds of sites for the B ions: the corner-sharing octahedral site and the face-sharing octahedral site. Generally, the B site ion with a low oxidation state and a large size occupies the former kind of site, and that with a high oxidation state and a small size occupies the latter kind of site. In the case of $Ba_3LnRu_2O_9$, Ln and Ru ions occupy the corner-sharing and face-sharing sites, respectively, and form the LnO_6 octahedron and the Ru_2O_9 polyhedron. This Ru_2O_9 polyhedron consists of two face-sharing RuO_6 octahedra and is called "Ru_2O_9 dimer". The magnetic behavior of this Ru_2O_9 dimer is attractive because of a very short Ru–Ru distance (2.5–2.7 Å) in the dimer. Therefore, one expects to find a strong magnetic interaction between Ru ions in the dimer, i.e., the formation of a magnetic dimer.

Previously, it was reported that the magnetic susceptibilities of $Ba_3M^{2+}Ru^{5+}{}_2O_9$ (M = Mg, Ca, Cd, and Sr) showed a broad maximum at 400–500 K and approached zero with decreasing temperature.[50] These features were explained by the antiferromagnetic coupling of Ru^{5+} ions in the dimer isolated magnetically by diamagnetic M^{2+} ions, which has the singlet ground state and the exchange integral $J = \sim -170$ K.[50,51]

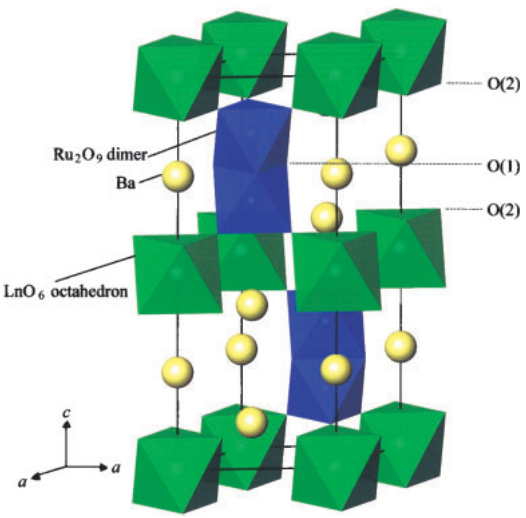

Fig. 18. The crystal structure of 6H-perovskite $Ba_3LnRu_2O_9$.

Since the most stable oxidation state of lanthanide ions is trivalent, the valence configuration expected for $Ba_3LnRu_2O_9$ is $Ba_3Ln^{3+}Ru^{4.5+}{}_2O_9$. If the magnetic moments of Ru ions in the dimer couple antiferromagnetically, each dimer has one unpaired electron at sufficiently low temperatures. In addition, if the lanthanide ions are magnetic, there exists a 180° Ru–O–Ln superexchange magnetic interaction. Therefore, this series of $Ba_3LnRu_2O_9$ compounds is likely to show interesting magnetic behavior due to the Ru_2O_9 dimer itself and the magnetic interaction between Ru and Ln ions.

Synthesis and Crystal Structures of $Ba_3LnRu_2O_9$. Polycrystalline samples of $Ba_3LnRu_2O_9$ were prepared by the conventional solid-state reaction. As starting materials, $BaCO_3$, RuO_2, Ln_2O_3 (Ln = Y, La, Nd, Sm–Gd, Dy–Lu), CeO_2, Pr_6O_{11}, and Tb_4O_7 were used. Before use, La_2O_3 and Nd_2O_3 were dried in air at 1173 K for a day. The samples were weighed in an appropriate metal ratio and well mixed in an agate mortar. The mixtures were pressed into pellets and then calcined at 1173 K for 12 h. The calcined materials were fired in air at 1373–1573 K for 60–108 h with several interval grindings and pelletings. The heating rate was 100 K/h. The progress of the reaction was monitored by powder X-ray diffraction measurements.

The results of the X-ray diffraction measurements show that $Ba_3LnRu_2O_9$ (Ln = Y, La–Nd, Sm–Lu) are formed as single-phase materials. The X-ray diffraction pattern of the Y compound is shown in Fig. 19. The Rietveld analyses of these diffraction data indicate that their crystal structures are a 6H-perovskite structure with space group $P6_3/mmc$ (No. 194). This result agrees with the results of previous structural studies.[52–54] The cation sites within the face-sharing octahedra of this structure are occupied by Ru ions and those within the corner-sharing octahedra are occupied by Ln ions. Neither any cation disorder between these two sites nor any oxygen defect were found within the error limits of these analyses.

The variation of lattice parameters for $Ba_3LnRu_2O_9$ with the ionic radius of Ln^{3+} is shown in Fig. 20. The lattice parameters for $Ba_3LnRu_2O_9$ increase monotonously with the ionic radius of Ln^{3+} from Lu to La, while those for the Ce, Pr and Tb compounds deviate substantially from this trend.[55] Figure 21(a) plots the variation of the refined Ln–O(2) bond lengths with the ionic radius of Ln^{3+}. Except for the Ce, Pr and Tb compounds, it is found that the Ln–O(2) bond length increases

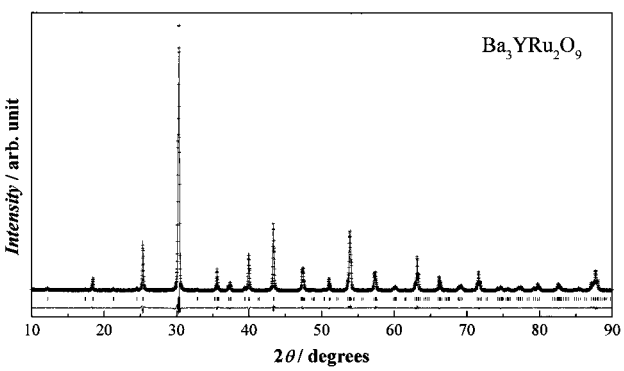

Fig. 19. X-ray diffraction pattern of $Ba_3YRu_2O_9$.

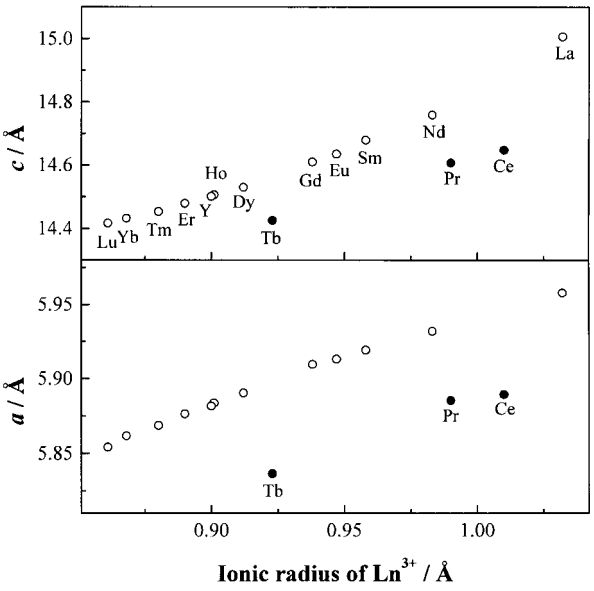

Fig. 20. Variation of lattice parameters for $Ba_3LnRu_2O_9$ with the Ln^{3+} ionic radius.

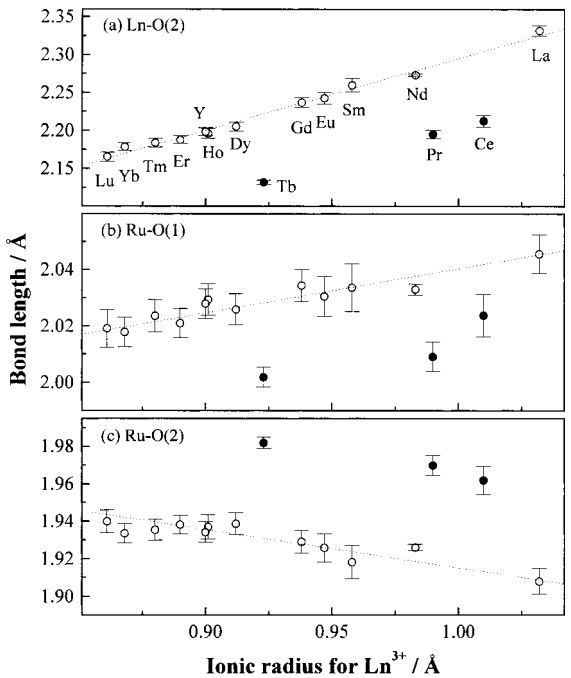

Fig. 21. Variation of (a) Ln–O(2), (b) Ru–O(1) and (c) Ru–O(2) bond lengths with the Ln^{3+} ionic radius.

with the ionic radius of Ln^{3+}. The refined Ce–O, Pr–O and Tb–O bond lengths are 2.213(8), 2.195(5) and 2.132(3) Å, respectively. They are close to Ln^{4+}–O^{2-} lengths calculated from Shannon's ionic radii:[56] 2.27 (for Ce), 2.25 (for Pr) and 2.16 Å (for Tb). These results indicate that the Ce, Pr and Tb ions are in the tetravalent state.

Figures 21(b) and (c) show the variation of the Ru–O(1) and Ru–O(2) bond lengths with the ionic radius of Ln^{3+}. The O(1) atoms are on the shared-face in the Ru_2O_9 dimer, and O(2) atoms are on the top or bottom face of the Ru_2O_9 dimer. The Ru–O(1) and Ru–O(2) bond lengths are 2.002–2.046 Å and 1.908–1.982 Å, respectively, indicating that two octahedra in this Ru_2O_9 dimer are distorted in shape. The Ru–O(1) length increases with increasing the ionic radius of Ln^{3+}, while the Ru–O(2) length decreases; such a tendency clearly indicates that the shape of Ru_2O_9 dimers becomes more distorted with increasing the ionic radius of Ln^{3+}.

For the Ce, Pr and Tb compounds, the Ru–O(1) and Ru–O(2) bond lengths deviate substantially from this trend. The average Ru–O bond lengths of these three compounds are 1.989–1.993 Å. The ruthenium ions are most likely tetravalent in the Ce, Pr, and Tb compounds, because the obtained lengths are very close to the Ru^{4+}–O^{2-} lengths found in other perovskites, for example, $CaRuO_3$: 1.99 Å,[57,58] $SrRuO_3$: 1.984 Å,[57,59] and $BaRuO_3$: 1.993 Å.[60] These results indicate that the valence configuration for $Ba_3LnRu_2O_9$ (Ln = Ce, Pr, Tb) is $Ba_3Ln^{4+}Ru^{4+}{}_2O_9$. On the other hand, the average Ru–O bond lengths of the other compounds with the Ln^{3+} ions are 1.971–1.985 Å. Such lengths are shorter than those of the Ce, Pr, and Tb compounds and longer than Ru^{5+}–O^{2-} length (1.965 Å) found in $Ba_3M^{2+}Ru^{5+}{}_2O_9$ (M = Zn and Ni).[61] This fact indicates that the average valency of Ru ions is +4.5, as is expected from the trivalent oxidation state of Ln ions and the stoichiometry in the oxygen content.

The difference in the interatomic distance between two ruthenium ions in the Ru_2O_9 dimer supports the above discussion. The Ru–Ru distance increases with the average valence of Ru ions in the $Ba_3MRu_2O_9$-type compounds: 2.481–2.515 Å for Ru^{4+} ions,[54,55,62] 2.517–2.582 Å for $Ru^{4.5+}$ ions,[53,54,62–67] and 2.649–2.701 Å for Ru^{5+} ions.[50,61,64,68,69] This tendency is explained by the difference in the strength of the electrostatic repulsion between ruthenium ions.

Electrical Resistivity of $Ba_3LnRu_2O_9$. The resistivity of $Ba_3LnRu_2O_9$ (Ln = Y, Lu) is plotted as a function of reciprocal temperature in Fig. 22(a). All the $Ba_3LnRu_2O_9$ compounds are nonmetallic at least in the range $100 < T < 400$ K, showing the increasing resistance with decreasing temperature.[55,63] Attempts to fit the observed data to a simple Arrhenius model were unsuccessful. The Mott variable-range hopping (VRH) model,[70]

$$\rho \propto \exp((T_0/T)^v), \tag{5}$$

was taken into account. When the parameter v is 1/3, experimental data show good linearity (Fig. 22(b)). The resistivity of the isostructural compounds $Ba_3MRu_2O_9$ (M = Fe, Co, Ni, Cu, and In) was reported previously, and it was found that the plots of $\log \rho$ vs $T^{-1/3}$ are linear.[71] Our results also suggest that the semiconducting behavior of $Ba_3LnRu_2O_9$ may be attributable to the variable-range hopping in two dimensions.[70] The crystal structure of $Ba_3LnRu_2O_9$ can be expressed by the alternate stacking of two kinds of two-dimensional layers which consist of the LnO_6 octahedra or the Ru_2O_9 polyhedra. This structural feature may account for the observed resistivity behavior.

Magnetic Properties of $Ba_3LnRu_2O_9$ (Ln = Y, La, Sm, Eu, Lu). In order to make clear the magnetic behavior of the Ru ions in the 6H-perovskites $Ba_3Ln^{3+}Ru^{4.5+}{}_2O_9$, the magnetic properties of $Ba_3LnRu_2O_9$ with Ln = Y, La, Sm, Eu, and Lu,[63] in which the Ln^{3+} ions are nonmagnetic or weak

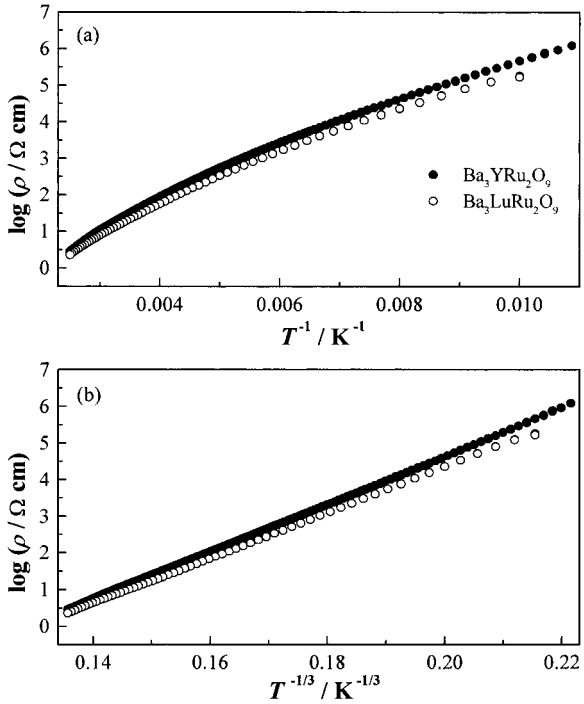

Fig. 22. Temperature dependence of the resistivity for $Ba_3LnRu_2O_9$ (Ln = Y and Lu). (a) $\log \rho$ vs T^{-1} plot; (b) $\log \rho$ vs $T^{-1/3}$ plot.

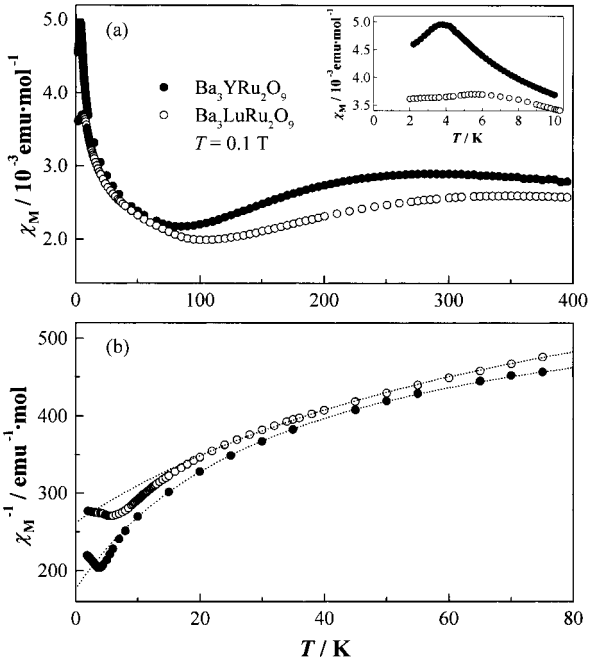

Fig. 23. Temperature dependence of (a) the magnetic susceptibility and (b) the reciprocal magnetic susceptibility for $Ba_3LnRu_2O_9$ (Ln = Y and Lu). The inset of Fig. 23(a) shows the detailed susceptibilities below 10 K. The broken lines in Fig. 23(b) show the fitting results by the modified Curie–Weiss law (see text).

magnetic, were studied. The Ru ions occupy the face-sharing octahedral sites (Ru_2O_9 dimer) and have a valence state of +4.5. When this $Ru^{4.5+}{}_2O_9$ dimer adopts a charge configuration of $Ru^{4+}Ru^{5+}O_9$, the total spin of a dimer may be $S = 1/2$. In that case, it is expected that not only the intra-dimer magnetic interaction but also the interaction between the dimers contribute to the magnetic properties of $Ba_3Ln^{3+}Ru^{4.5+}{}_2O_9$.

The temperature dependence of the magnetic susceptibilities for $Ba_3YRu_2O_9$ and $Ba_3LuRu_2O_9$ is plotted in Fig. 23(a). None of these compounds obey the Curie–Weiss law. They show a broad maximum at 290 K (for Ln = Y), 180 K (Sm), 135 K (Eu), and 345 K (Lu). The magnetic susceptibility of $Ba_3LaRu_2O_9$ shows a plateau around 22 K. In addition, they show another magnetic anomaly at low temperatures: 4.5 K (for Ln = Y), 6.0 K (La), 12.5 K (Sm), 9.5 K (Eu), and 9.5 K (Lu).

The observed broad maxima above 100 K are similar to those found in the magnetic susceptibility vs temperature curves for $Ba_3M^{2+}Ru^{5+}{}_2O_9$ (M^{2+}: nonmagnetic ions; M = Mg, Ca, Sr, and Cd) reported by Darriet et al.[50] They explained this behavior by using a dimer model, in which two spins of Ru^{5+} ions in the Ru_2O_9 dimer couple antiferromagnetically. Figure 23(b) shows the variation of the reciprocal magnetic susceptibilities against temperature for the present $Ba_3YRu_2O_9$ and $Ba_3LuRu_2O_9$ in the temperature range of 1.8 to 80 K. Since a large temperature-independent contribution to the susceptibility is observed, the data are treated in terms of the modified Curie–Weiss law:

$$\chi = C/(T - \theta) + \chi_{TIP}. \quad (6)$$

In the temperature range above 20 K, applying this modified Curie–Weiss law to the temperature dependence of the susceptibilities gives $\mu_{eff} = 0.57\ \mu_B$, $\theta = -10.2$ K, $\chi_{TIP} = 1.7 \times 10^{-3}$ emu mol^{-1} for $Ba_3YRu_2O_9$, and $\mu_{eff} = 0.77\ \mu_B$, $\theta = -31.0$ K, $\chi_{TIP} = 1.4 \times 10^{-3}$ emu mol^{-1} for $Ba_3LuRu_2O_9$. The magnitude of the effective magnetic moment indicates that each Ru_2O_9 dimer has one unpaired electron. The negative Weiss constants show that the magnetic interaction between the Ru_2O_9 dimers is antiferromagnetic.

Figure 24(a) shows the variation of the specific heat divided by temperature (C_p/T) for $Ba_3YRu_2O_9$ and $Ba_3LuRu_2O_9$ as a function of temperature. An anomaly has been observed for each compound, which corresponds to the anomaly found at low temperatures in the magnetic susceptibility. The temperature dependence of the total entropy, which is calculated by $S_{total} = \int C_p/T\, dT$, is shown in Fig. 24(b). The magnetic entropy change derived from this magnetic anomaly for $Ba_3YRu_2O_9$ and $Ba_3LuRu_2O_9$ is estimated to be ~3.0 J mol^{-1} K^{-1}. These magnetic entropy changes correspond to the antiferromagnetic orderings of $Ru^{4.5+}{}_2O_9$ dimers with $S = 1/2$. The value of 3.0 J mol^{-1} K^{-1} is smaller than the expected value $R\ln(2S + 1) = R\ln 2 = 5.76$ J mol^{-1} K^{-1}. This may be due to the occurrence of the short-range magnetic ordering at temperatures higher than the respective magnetic transition temperatures.

Magnetic Properties of $Ba_3LnRu_2O_9$ (Ln = Gd, Ho–Yb). The magnetic properties of 6H-perovskites $Ba_3Ln^{3+}Ru^{4.5+}{}_2O_9$ with Ln = Gd, Ho–Yb[67] are discussed. These lanthanide ions have large magnetic moments. So, the Ln ions should greatly contribute to the magnetic properties of $Ba_3LnRu_2O_9$. In the case that both the Ru and Ln ions are magnetic, these compounds may show magnetic cooperative phenomena due to

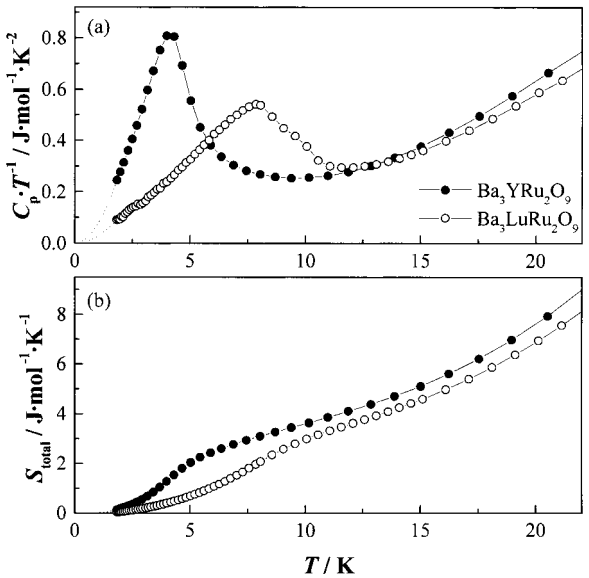

Fig. 24. Temperature dependence of (a) the specific heat divided by temperature and (b) total entropy for $Ba_3LnRu_2O_9$ (Ln = Y and Lu).

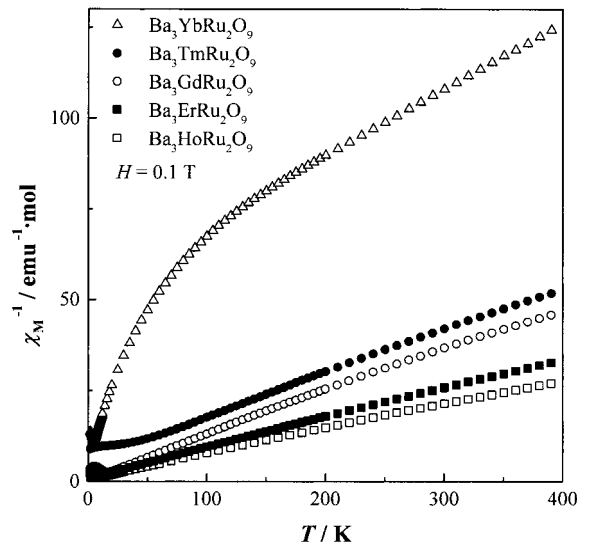

Fig. 25. Temperature dependence of reciprocal magnetic susceptibilities for $Ba_3LnRu_2O_9$ (Ln = Gd, Ho–Yb).

the interaction between d and f electrons at sufficiently low temperatures.

The temperature dependence of reciprocal magnetic susceptibilities for $Ba_3LnRu_2O_9$ (Ln = Gd, Ho–Yb) is shown in Fig. 25. The susceptibility data in the higher temperature region ($T > 150$ K) are fitted with the Curie–Weiss law; the effective magnetic moments μ_{eff} and Weiss constants θ are listed in Table 4. The Weiss constants are negative; therefore, the predominant magnetic interactions in these compounds are antiferromagnetic. The effective magnetic moments are obviously closer to those for the free Ln^{3+} ions ($\mu_{Ln^{3+}}$) rather than to the values calculated from

$$\mu_{cal} = \sqrt{\mu_{Ln^{3+}}{}^2 + \mu_{Ru^{4+}}{}^2 + \mu_{Ru^{5+}}{}^2}. \quad (7)$$

Table 4. The Magnetic Moments for Free Ln^{3+} Ion ($\mu_{Ln^{3+}}$), Calculated Magnetic Moments for All Ions (μ_{cal}), Effective Magnetic Moments (μ_{eff}) and Weiss Constants (θ) for $Ba_3LnRu_2O_9$ (Gd, Ho–Yb)

Ln^{3+}	$\mu_{Ln^{3+}}/\mu_B$	μ_{cal}/μ_B	μ_{eff}/μ_B	θ/K
Gd^{3+}	7.94	9.28	7.68(1)	−2.9(5)
Ho^{3+}	10.58	11.62	10.15(1)	−5.4(4)
Er^{3+}	9.59	10.72	9.45(2)	−9.9(7)
Tm^{3+}	7.55	8.94	7.35(1)	−24.5(5)
Yb^{3+}	4.54	6.60	5.26(1)	−178(2)

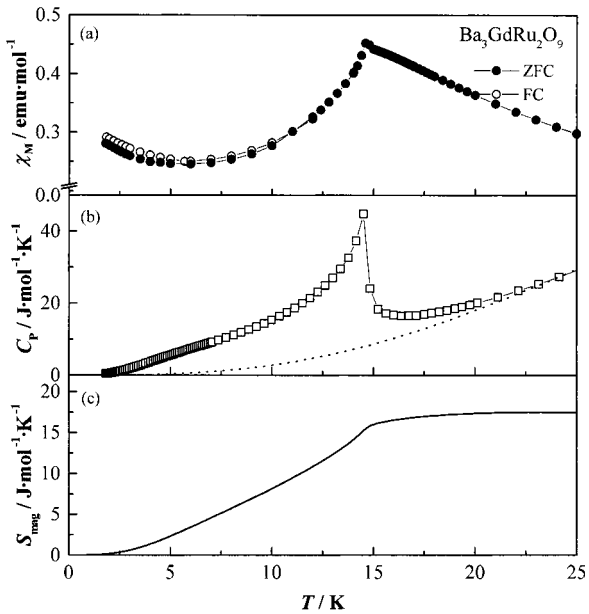

Fig. 26. Temperature dependence of (a) the magnetic susceptibility, (b) specific heat and (c) magnetic entropy of $Ba_3GdRu_2O_9$.

This fact indicates that the contribution of Ru ions to the effective magnetic moment is very small. Therefore, the Ru ions should no longer be in the paramagnetic state in this temperature range, i.e., the magnetic moments of two Ru ions in each Ru_2O_9 dimer are coupled antiferromagnetically. The similar antiferromagnetic coupling has been found in the analogous 6H-perovskites $Ba_3LnRu_2O_9$ (Ln = nonmagnetic or weak magnetic ions).

Figures 26(a) and 27(a) show the temperature dependence of the magnetic susceptibility for $Ba_3GdRu_2O_9$ and $Ba_3HoRu_2O_9$ at low temperatures. It is found that the materials show magnetic anomalies at 14.8 K (Ln = Gd) and 10.2 K (Ho). Figures 26(b) and 27(b) show the variation of the specific heats as a function of temperature. The specific heat of any compound shows a λ-type anomaly at the same temperature at which the magnetic anomaly is observed in the susceptibility vs temperature curve. This result indicates that these anomalies are an antiferromagnetic transition.

The specific heat mainly consists of the lattice, electronic, and magnetic specific heats. Specific heat data for the suitable diamagnetic $A_3MM'_2O_9$ compounds which are isomorphous with $Ba_3GdRu_2O_9$ and $Ba_3HoRu_2O_9$ are not available. Then, in order to estimate the lattice and electronic contributions, we

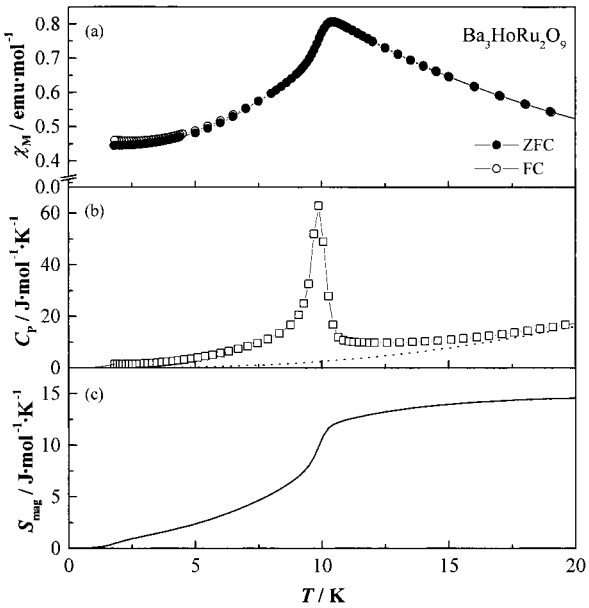

Fig. 27. Temperature dependence of (a) the magnetic susceptibility, (b) specific heat and (c) magnetic entropy of $Ba_3HoRu_2O_9$.

used a polynomial function of the temperature, $f(T) = aT^3 + bT^5 + cT^7$, in which the constants were determined by fitting this function to the specific heat data observed between 20 and 40 K. Each calculated curve is shown in Fig. 26(b) and 27(b) as a dotted curve. The magnetic specific heat (C_{mag}) for $Ba_3GdRu_2O_9$ and $Ba_3HoRu_2O_9$ is obtained by subtracting the lattice and electronic contributions from the total specific heat, i.e., $C_{mag}(T) = C_p(T) - f(T)$.

The temperature dependence of the magnetic entropy calculated by $S_{mag} = \int C_{mag}/T \, dT$ is shown in Figs. 26(c) and 27(c). Since the magnetic entropy changes are very large compared with those for $Ba_3YRu_2O_9$ and $Ba_3LuRu_2O_9$ ($\Delta S_{mag} = \sim 3.0$ J mol^{-1} K^{-1}), the magnetic transitions observed for these $Ba_3LnRu_2O_9$ compounds are due to the magnetic ordering of Ln^{3+} ions. The magnetic entropy change associated with the antiferromagnetic ordering for $Ba_3GdRu_2O_9$ is 17.5 J mol^{-1} K^{-1} (Fig. 26(c)); this value is close to $R \ln W = R \ln 8 = 17.3$ J mol^{-1} K^{-1}. This result is consistent with the fact that the ground state for Gd^{3+} ion is $^8S_{7/2}$ (the degeneracy of which is $W = 2S + 1 = 8$) and confirms that the magnetic anomaly at 14.8 K is due to the antiferromagnetic ordering of Gd^{3+} ions. The magnetic entropy change for $Ba_3HoRu_2O_9$ is 14.7 J mol^{-1} K^{-1} (Fig. 27(c)). In an octahedral crystal field environment, the ground state of $^5I_8$ for the Ho^{3+} ion is a singlet state Γ_1 or a doublet state Γ_3, and there exists a low lying excited state (Γ_4; triplet).[29] If these three states degenerate or if the energy difference among them is very small, the expected entropy change due to the Ho^{3+} antiferromagnetic transition is $R \ln 6 = 14.9$ J mol^{-1} K^{-1}.

Magnetic Properties of $Ba_3LnRu_2O_9$ (Ln = Ce, Pr, Tb). The 6H-perovskites $Ba_3LnRu_2O_9$ with Ln = Ce, Pr, or Tb[55] have a valence configuration of $Ba_3Ln^{4+}Ru^{4+}{}_2O_9$. In this case, the magnetic interactions between two Ru^{4+} ions in the $Ru^{4+}{}_2O_9$ dimer and those between the Ru^{4+} and Ln^{4+} ions operate.

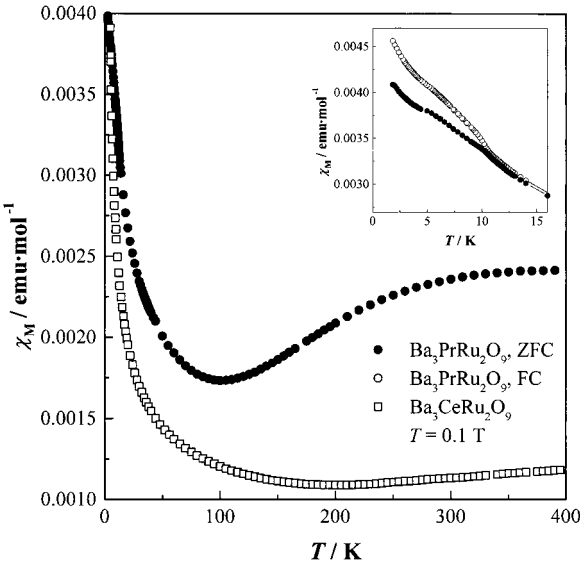

Fig. 28. Temperature dependence of magnetic susceptibilities for $Ba_3LnRu_2O_9$ (Ln = Ce and Pr). The inset shows the detailed susceptibilities below 16 K.

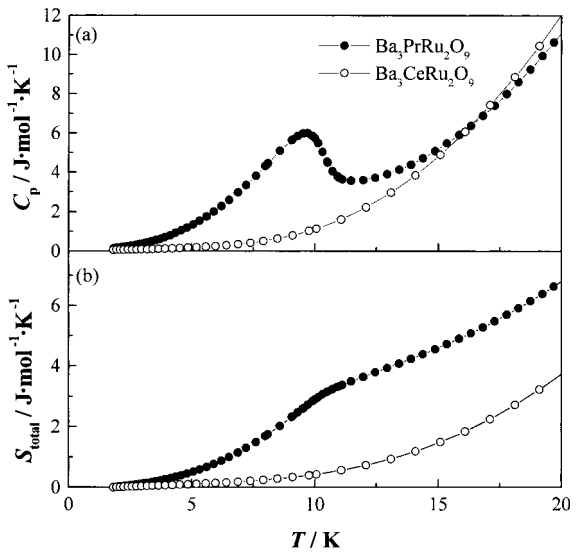

Fig. 29. Temperature dependences of (a) the specific heat and (b) the total entropy for $Ba_3LnRu_2O_9$ (Ln = Ce and Pr).

The temperature dependence of the magnetic susceptibilities for $Ba_3CeRu_2O_9$ and $Ba_3PrRu_2O_9$ is plotted in Fig. 28. The susceptibilities gradually increase with temperature above 200 K and 100 K, respectively. These features are due to the magnetic interaction between Ru^{4+} ions in the $Ru^{4+}{}_2O_9$ dimers with a singlet ground state, $S = 0$. For $Ba_3PrRu_2O_9$, an anomaly at 10.5 K in the temperature dependence of susceptibilities and the divergence between the ZFC and FC susceptibilities (see the inset of Fig. 28) is observed below this temperature. Figure 29(a) shows the variation of the specific heat for $Ba_3CeRu_2O_9$ and $Ba_3PrRu_2O_9$ as a function of temperature. The specific heat for $Ba_3PrRu_2O_9$ shows a λ-type anomaly at 10.5 K, which corresponds to the magnetic anomaly found in the magnetic susceptibilities. This fact indi-

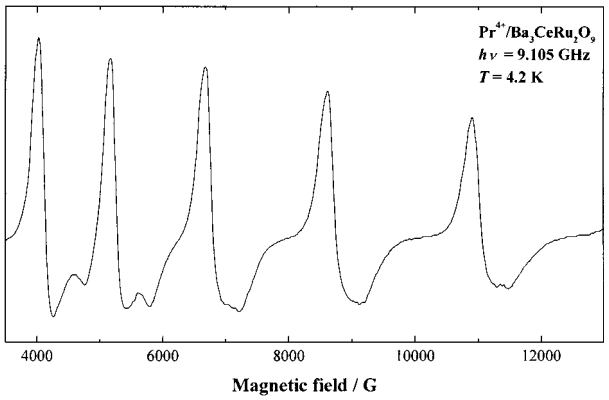

Fig. 30. EPR spectrum for Pr^{4+} ion doped in $Ba_3CeRu_2O_9$ measured at 4.2 K.

cates that an antiferromagnetic transition of Pr^{4+} ions occurs at this temperature. The temperature dependence of the total entropy for $Ba_3CeRu_2O_9$ and $Ba_3PrRu_2O_9$ has been calculated from the relation $S_{\text{total}} = \int C_p/T\,dT$, and it is shown in Fig. 29(b). The magnetic entropy change associated with the antiferromagnetic ordering for $Ba_3PrRu_2O_9$ is estimated by extracting the entropy of $Ba_3CeRu_2O_9$ from that of $Ba_3PrRu_2O_9$; it is $\sim$3.2 J mol^{-1} K^{-1} at 15 K. The ground state $^2F_{5/2}$ of the Pr^{4+} ion is split into a doublet (Γ_7) and a quartet (Γ_8) in the octahedral symmetry. The magnetic entropy change of $Ba_3PrRu_2O_9$ is closer to $R\ln 2 = 5.76$ J mol^{-1} K^{-1} rather than $R\ln 4 = 11.53$ J mol^{-1} K^{-1}, which indicates that the ground state is Γ_7.

Since the praseodymium ion in the $Ba_3PrRu_2O_9$ is tetravalent, an EPR spectrum should be observed because the Pr^{4+} ion is a Kramers ion ([Xe]4f^1 configuration). In order to measure its EPR spectrum, we have prepared a sample in which the $Ba_3PrRu_2O_9$ is diluted with isomorphous $Ba_3CeRu_2O_9$. No EPR spectra were observed at room temperature. At low temperatures, EPR spectra could be observed. Figure 30 shows the spectrum measured at 4.2 K. This observation of an EPR spectrum strongly indicates that the oxidation state of the praseodymium ion is not trivalent, but tetravalent, because the non-Kramers Pr^{3+} ion usually shows no EPR spectrum.[72] Five absorption lines were observed. They are due to the hyperfine interaction with the nuclear spin for ^{141}Pr ($I = 5/2$) (natural abundance 100%). Since the nuclear spin for ^{141}Pr is 5/2, the number of EPR absorption lines due to the hyperfine interaction should be six. However, the number of measured absorption lines is not six, but five; the sixth absorption line was not observed in this experiment. The spacings between EPR absorption lines become wider with greater resonance magnetic field, which indicates that the electron spin quantum number and the nuclear spin quantum number are not good quantum numbers. To analyze this EPR spectrum, the spin Hamiltonian including the electronic Zeeman term and the hyperfine term must be solved exactly. The solution is well known (Breit–Rabi equation) and has been given by Ramsey[73] and others.[74] The g value and hyperfine coupling constant were determined by fitting the spin Hamiltonian to the observed EPR spectrum.[75] The best fit parameters are $|g| = 0.694$ and $A = 0.0604$ cm^{-1}. The resonance field for the sixth transition (the highest resonance field) is 13615 G,

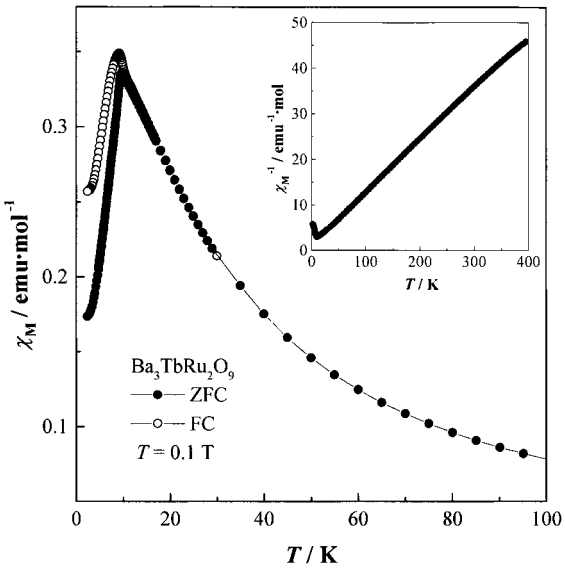

Fig. 31. Temperature dependence of the magnetic susceptibility for $Ba_3TbRu_2O_9$. The inset shows the reciprocal susceptibility vs temperature curve.

which is beyond our maximum obtainable magnetic field. The measured g value is much smaller than $|-10/7|$,[76] which shows that the crystal field effect on the behavior of a 4f electron is large.

The temperature dependence of the magnetic susceptibility and specific heat for $Ba_3TbRu_2O_9$ is plotted in Fig. 31. The susceptibility shows a maximum at 9.5 K and decreases rapidly with decreasing temperature below this temperature, indicating the occurrence of an antiferromagnetic transition. Below the transition temperature, the ZFC and FC susceptibilities diverge. The higher temperature data ($T > 20$ K) can be fitted using the Curie–Weiss law (see the inset of Fig. 31). The obtained effective magnetic moment and Weiss constant are 7.93(1) μ_B and $-2.8(3)$ K, respectively. This effective magnetic moment is closer to that for Tb^{4+} ions (7.94 μ_B) rather than that for Tb^{3+} ions (9.72 μ_B), showing that the terbium ion is in the tetravalent state. The specific heat shows a λ-type anomaly at 9.5 K, which corresponds to the magnetic anomalies found in the magnetic susceptibilities.[55] The neutron diffraction measurements were carried out above and below this transition temperature (Fig. 32). The data collected at 2 K show a number of low angle peaks, which are not observed at 15 K. They are the magnetic reflections due to an antiferromagnetic ordering of the Tb^{4+} ions. They are indexed in the crystallographic unit cell with odd values of l; however, the (001) peak ($2\theta = \sim 7.2^\circ$) and other (00l) peaks are negligibly weak. These facts indicate that the Tb^{4+} ions have antiparallel magnetic moments with each other, and that the direction of ordered moments is parallel to the c axis. The magnetic structure of $Ba_3TbRu_2O_9$ is illustrated in Fig. 33. In this magnetic structure, the magnetic moments of the Tb^{4+} ions order ferromagnetically in the xy plane, and these ferromagnetic sheets are stacked antiferromagnetically along the c axis. The ordered magnetic moment of Tb^{4+} ions is 6.84(4) μ_B. This value is reasonable for Tb^{4+} (4f^7) and comparable to those of other perovskites containing Tb^{4+} ions: 6.76 μ_B

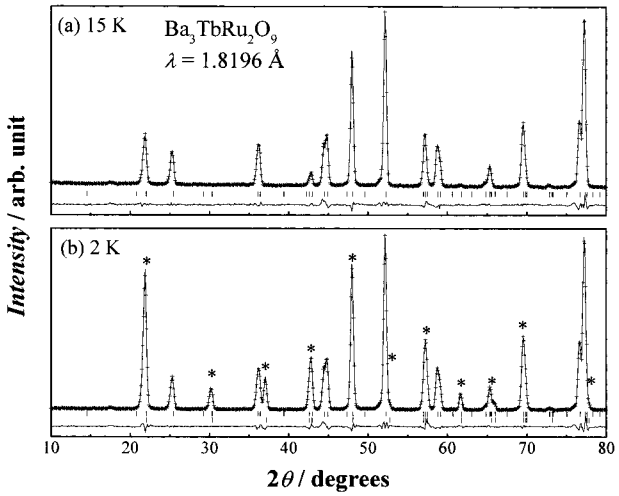

Fig. 32. Powder neutron diffraction profiles of $Ba_3TbRu_2O_9$ at (a) 15 K and (b) 2 K. Marked (∗) peaks indicate the magnetic reflections.

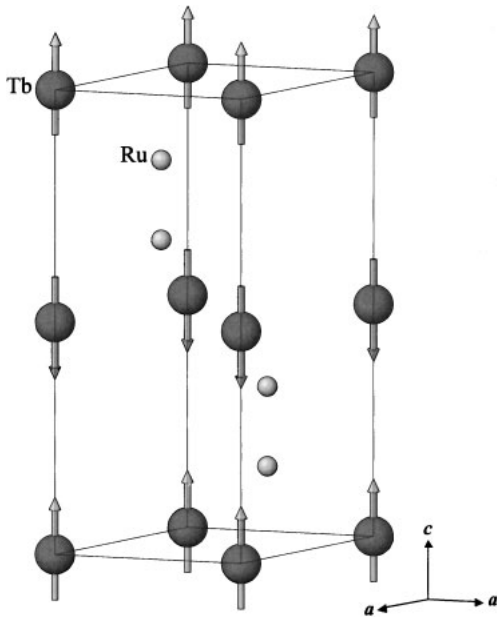

Fig. 33. Magnetic structure of $Ba_3TbRu_2O_9$. Diamagnetic ions are omitted. The arrows indicate the direction of the magnetic moments.

($SrTbO_3$) and 6.5 μ_B ($BaTbO_3$) at 10 K.[13]

Structural and Magnetic Transition of $Ba_3NdRu_2O_9$. The crystal structure and magnetic properties of $Ba_3Nd^{3+}Ru^{4.5+}{}_2O_9$[66] are very peculiar among a series of $Ba_3LnRu_2O_9$ compounds, i.e., the structural phase transition and ferromagnetic transition have been observed only in this compound.

Neutron diffraction data collected at room temperature indicate that $Ba_3NdRu_2O_9$ is formed as a single phase and adopts a 6H-perovskite structure with space group $P6_3/mmc$. Neutron diffraction measurements were also performed at 10, 60, and 180 K to check whether the crystal phase transition occurred or not, and to determine the crystal structures at low temperatures. Their diffraction profiles are shown in Fig. 34. The crystal structure at 180 K is the same as that at

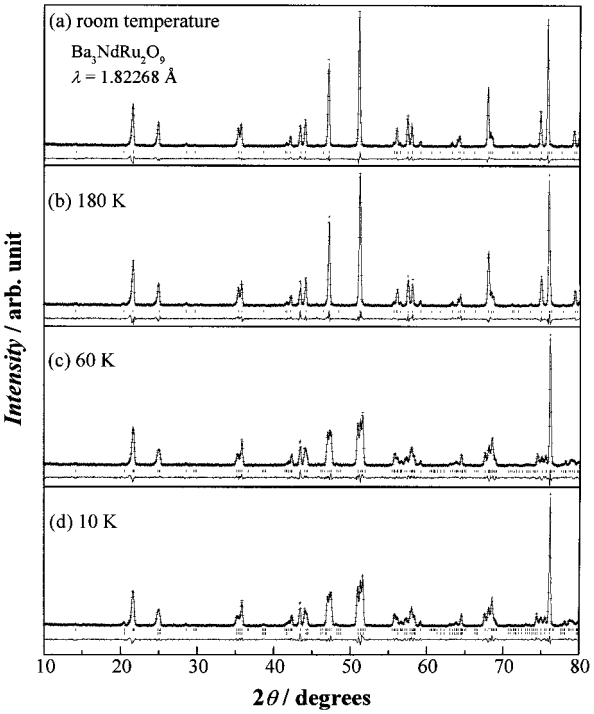

Fig. 34. Powder neutron diffraction profiles of $Ba_3NdRu_2O_9$ at various temperatures.

room temperature (space group $P6_3/mmc$). The diffraction data collected at 10 and 60 K indicate that the crystal structures at these temperatures have a lower symmetry than that at 180 K. It has been found that the analysis using a structure model, which has a monoclinic symmetry with space group $C2/c$ (No. 15), gives a good agreement with experimental data. The crystal structure of $Ba_3NdRu_2O_9$ at 60 K is illustrated in Fig. 35. The unit cell parameters ($a_{mono} \approx a_{hex}$, $b_{mono} \approx \sqrt{3}b_{hex}$, $c_{mono} \approx c_{hex}$ and β_{mono}) at 60 K are 5.9173(3), 10.2425(5), 14.7663(9) Å, and 90.819(2)°, respectively. The neutron diffraction profile at 10 K indicates that there exist some magnetic reflection peaks due to a ferromagnetic ordering of Nd^{3+} ions. The crystal structure at 10 K has the same symmetry as that at 60 K.

Powder X-ray diffraction measurements have been also performed in the temperature range of 13 to 200 K. The diffraction profiles collected at 13–110 K are indexed in a monoclinic unit cell ($C2/c$), and those collected at 130–200 K are indexed in a hexagonal unit cell ($P6_3/mmc$). Therefore, it is considered that the structural phase transition occurs around 120 K.

The temperature dependence of the magnetic susceptibility (M/H) of $Ba_3NdRu_2O_9$ is plotted in Fig. 36. The magnetic susceptibility shows a rapid increase when the temperature is decreased through 24 K, and a large divergence between the ZFC and FC susceptibilities is found below this temperature. These results indicate that a ferromagnetic or a ferrimagnetic transition has occurred at 24 K. The temperature dependence of the reciprocal susceptibility (H/M) is shown in the inset of Fig. 36. A linear relationship between the reciprocal susceptibility vs temperature is observed above 120 K. Below this temperature, the susceptibility deviates from this relationship, which is due to the structural phase transition. The higher tem-

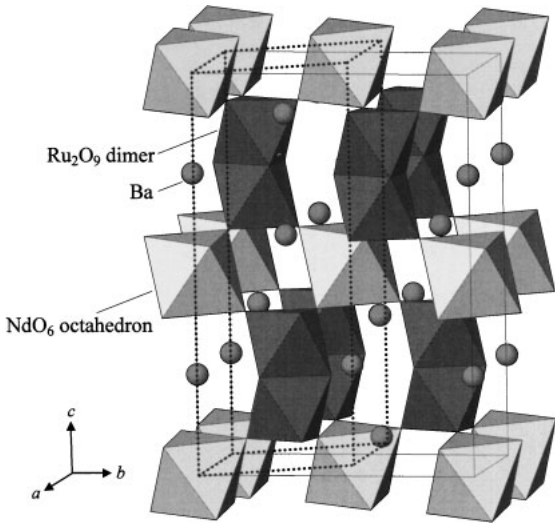

Fig. 35. The crystal structure of $Ba_3NdRu_2O_9$ at 60 K. The dashed lines indicate the hexagonal unit cell.

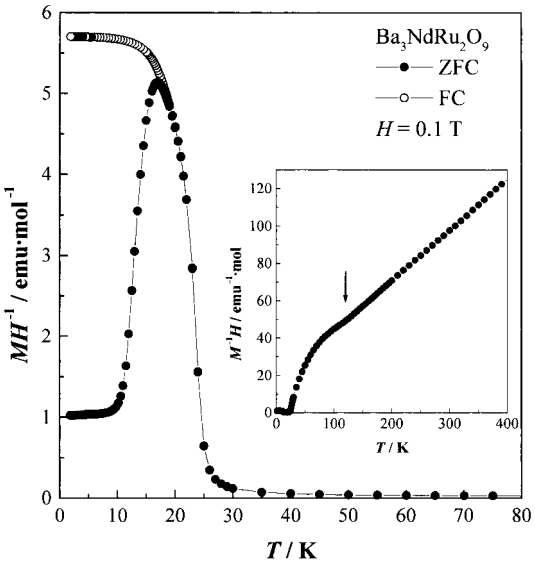

Fig. 36. Temperature dependence of the magnetic susceptibility for $Ba_3NdRu_2O_9$ at low temperatures. The inset shows the reciprocal susceptibility vs temperature curve. An arrow shows the phase transition temperature (see text).

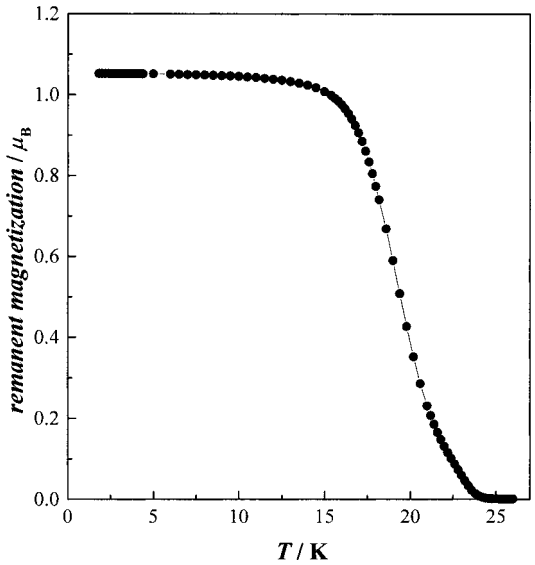

Fig. 37. Temperature dependence of the remanent magnetization of $Ba_3NdRu_2O_9$.

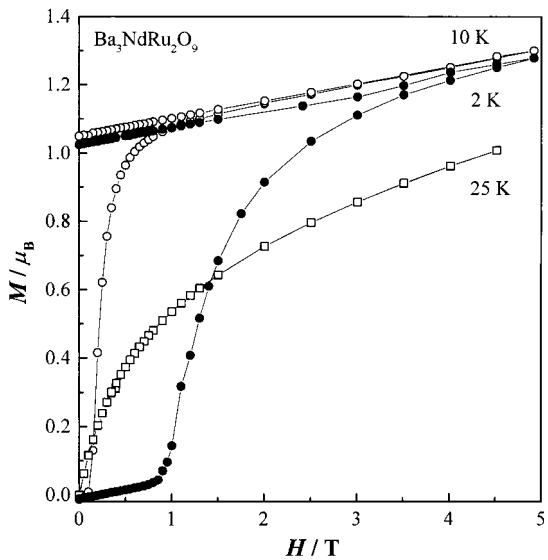

Fig. 38. Field dependence of the magnetization of $Ba_3NdRu_2O_9$ at 2, 10, and 25 K.

perature data ($T > 200$ K) are fitted by using the Curie–Weiss law. The obtained effective magnetic moment and Weiss constant are 5.82(3) μ_B and $-85(3)$ K, respectively. The temperature dependence of the remanent magnetization is plotted in Fig. 37. The remanent magnetization is constant ($\sim$1.05 μ_B) below 15 K and decreases with increasing temperature between 15 and 24 K. It is zero above 24 K. The field dependence of the magnetization measured at 2, 10, and 25 K is shown in Fig. 38. Data collected at 2 and 10 K show a hysteresis loop, which means that there exists a ferromagnetic moment.

Figure 39(a) shows the variation of the specific heat for $Ba_3NdRu_2O_9$ as a function of temperature. Two anomalies have been observed at 17 and 24 K. The λ-type anomaly at 24 K corresponds to the magnetic transition found in the magnetic susceptibility. The magnetic specific heat for $Ba_3NdRu_2O_9$ is obtained by subtracting the specific heat of a nonmagnetic 6H-perovskite $Ba_3SrNb_2O_9$ from that of $Ba_3NdRu_2O_9$. The temperature dependences of the magnetic specific heat divided by temperature (C_{mag}/T) and of the magnetic entropy (S_{mag}) are shown in Figs. 39(b) and 39(c). The magnetic entropy change (ΔS_{mag}) between 1.8 and 24 K is $\sim$11.1 J mol^{-1} K^{-1}. This value is the sum of the entropy changes for the anomalies at 17 and 24 K. It seems that the entropy changes of these anomalies are equal; in that case, each entropy change is very close to $R \ln W = R \ln 2 = 5.76$ J mol^{-1} K^{-1}. It is considered that they are due to the magnetic ordering of $Ru^{4.5+}{}_2O_9$ dimers ($S = 1/2$) and that of Nd^{3+} ions with a Kramers doublet ground state.

Now the magnetic structure of $Ba_3NdRu_2O_9$ will be

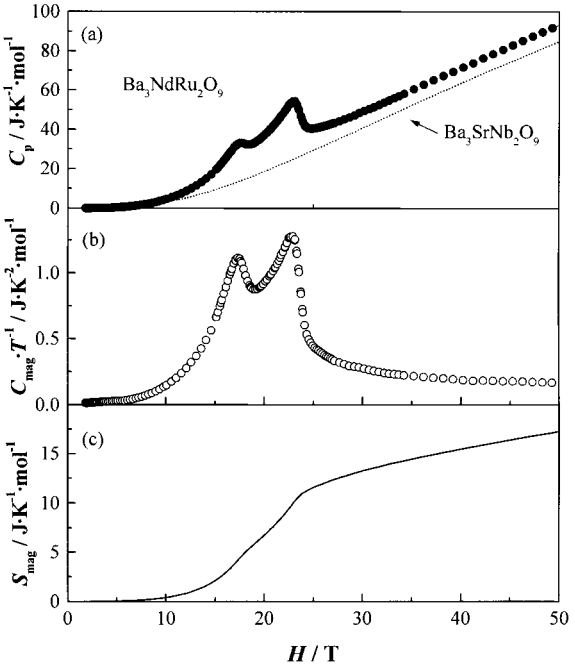

Fig. 39. Temperature dependence of (a) the specific heat, (b) the magnetic specific heat divided by temperature, and (c) magnetic entropy for $Ba_3NdRu_2O_9$. The dashed line in Fig. 39(a) shows the specific heat of nonmagnetic $Ba_3SrNb_2O_9$ (see text).

discussed. The neutron diffraction measurements at 10 K (Fig. 32(b)) show some magnetic reflection peaks. The positions of the magnetic diffraction lines are in accordance with those of the nuclear ones. The Rietveld analysis determines the magnetic structure which is illustrated in Fig. 40. In this magnetic structure, the magnetic moments of Nd^{3+} ions order ferromagnetically and are aligned along the *c*-axis. The ordered magnetic moment is 1.65(8) μ_B/Nd^{3+} ion.

Summary of 6H-Perovskites $Ba_3LnRu_2O_9$. The perovskite-related compounds $Ba_3LnRu_2O_9$ (Ln = Y, lanthanides) have the 6H-$BaTiO_3$-type structure with the space group $P6_3/mmc$. For the Ce, Pr, and Tb compounds, the oxidation states of both Ru and Ln ions are tetravalent, i.e., $Ba_3Ln^{4+}Ru^{4+}{}_2O_9$. On the other hand, the other compounds adopt a valence configuration of $Ba_3Ln^{3+}Ru^{4.5+}{}_2O_9$. Their magnetic properties vary widely with Ln ion, and are summarized in Table 5. In the $Ba_3LnRu_2O_9$ compounds, two kinds of the magnetic interactions are important for determining their magnetic properties. One is the magnetic interaction between two Ru ions in the Ru_2O_9 dimers; this brings about a strong antiferromagnetic coupling between the Ru ions, and the characteristic temperature-dependence of the magnetic susceptibilities (a broad maximum above ~100 K) is observed for $Ba_3LnRu_2O_9$ (Ln = nonmagnetic or weak magnetic lanthanide ions). Another important interaction is the one between the Ru and Ln ions via the linear Ru–O–Ln pathway, which is in common with the case of double perovskites A_2LnRuO_6. The magnetic transition due to the magnetic ordering of Ln ions has been found in the $Ba_3LnRu_2O_9$ compounds (Ln = magnetic ions). For the Nd and Tb compounds, the magnetic structures have been determined by the neutron diffraction measurements.

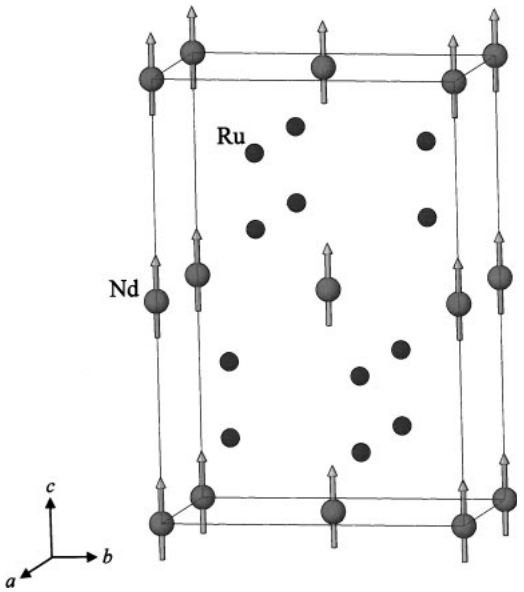

Fig. 40. Magnetic structure of $Ba_3NdRu_2O_9$. Diamagnetic ions are omitted. The arrows indicate the direction of the magnetic moments.

Table 5. The Magnetic Properties of 6H-Perovskites $Ba_3LnRu_2O_9$

Ln	Oxidation state of Ln ion	T_a/K	T_b/K	Ordered magnetic moment/μ_B	Ref.
Y	+3	290	4.5 (AF)	—	(63)
La	+3	22 (plateau)	6.0 (AF)	—	(63)
Ce	+4	>400	—	—	(55)
Pr	+4	>380	10.5 (AF)	—	(55)
Nd	+3	—	24.0 (F)	1.65/Nd^{3+} (10 K)	(66)
Sm	+3	180	12.5 (AF)	—	(63)
Eu	+3	135	9.5 (AF)	—	(63)
Gd	+3	—	14.8 (AF)	—	(67)
Tb	+4	—	9.5 (AF)	6.84/Tb^{4+} (2 K)	(55)
Dy	+3	—	27.8 (AF)	—	(77)
Ho	+3	—	10.2 (AF)	—	(67)
Er	+3	—	6.0 (AF)	—	(67)
Tm	+3	—	8.3 (AF)	—	(67)
Yb	+3	—	4.5 (AF)	—	(67)
Lu	+3	345	9.5 (AF)	—	(63)

Note. T_a: temperatures at which broad maxima are observed in the magnetic susceptibility vs temperature curves, T_b: magnetic transition temperatures, AF: antiferromagnetic, and F: ferromagnetic.

Conclusion

This account presents the solid-state chemistry of some perovskite-related oxides containing lanthanide ions. Their crystal structures and magnetic properties were investigated. The magnetic interactions between 4f electrons which characterize the magnetic properties of lanthanide ions are various and attractive. However, the 4f electrons are effectively shielded by the outer $5s^25p^6$ electron shells, which results in very weak magnetic interactions between 4f electrons. If one introduces the ruthenium ions as the d electron system and by achieving

the alternative arrangement of the lanthanide (4f) and ruthenium (4d) ions at the B-sites of the perovskite structure, the stronger magnetic interaction between f and d electrons becomes important.

For the double perovskites A_2LnRuO_6, antiferromagnetic transitions due to the magnetic cooperative phenomena between f and d electrons have been found at relatively high temperatures. In addition, if the number of 4f electrons changes, the systematical information concerning the d–f magnetic interaction can be obtained. For the 6H-perovskites $Ba_3LnRu_2O_9$, the peculiar temperature dependence of the magnetic susceptibilities has been observed. They have been explained by the d–f magnetic interaction and the magnetic coupling between Ru ions in the Ru_2O_9 dimer.

It is concluded that perovskite-related oxides containing both lanthanide and ruthenium ions show interesting magnetic properties, which originate from both the characteristics of each magnetic ion and the magnetic interaction between them. These studies should contribute to the total understanding of the magnetic properties of the d–f electron system. In order to deepen this understanding and to find more fascinating magnetic properties, a further investigation on compounds containing other metal ions such as 5d elements (osmium, rhenium, and iridium) and 5f elements (actinides) will be needed. Our study of such compounds is going on.

The results introduced in this article have been performed with many collaborators whose names appear in the references and who devoted themselves to the present study. Especially, the authors wish to thank Dr. M. Wakeshima (Lecturer of the Division of Chemistry, Hokkaido University) and Dr. K. Tezuka (Research Associate of the Department of Applied Chemistry, Utsunomiya University) for their collaboration, stimulating discussions and fruitful comments. We express our sincere gratitude to Dr. K. Matsuhira (Research Associate of Kyushu Institute of Technology), Dr. N. Taira (Research Associate of Gunma National College of Technology), Mr. D. Harada, Mr. K. Henmi, Ms. Y. Izumiyama, and Mr. Y. Sasaki for their collaboration in the Inorganic Chemistry Laboratory of Hokkaido University. The authors also thank Drs. A. Nakamura, Y. Ishii, Y. Shimojo and Y. Morii of Japan Atomic Energy Research Institute, and Dr. K. Ohoyama, Dr. A. Tobo and Professor Y. Yamaguchi of Tohoku University for their useful suggestions and many supports for the neutron diffraction measurements.

References

1 J. B. Goodenough, "Magnetism and the Chemical Bond," John Willy, New York (1963).

2 J. B. Goodenough and J. M. Longo, "Landolt-Börnstein," New Series, Vol. Ⅲ/4a, Springer, Berlin (1970).

3 J. B. Bednorz and K. A. Müller, *Z. Phys. B*, **64**, 189 (1986).

4 H. Iwahara, T. Esaka, H. Uchida, and N. Maeda, *Solid State Ionics*, **3**, 359 (1981).

5 L. E. Cross, "Ferroelectric Ceramics," Brikhauser Verlag, Basel (1993).

6 H. Kuwahara, Y. Tomioka, A. Asamitsu, Y. Morimoto, and Y. Tokura, *Science*, **270**, 961 (1995).

7 H. P. J. Wijn, "Binary Lanthanide Oxides" in "Landolt-Börnstein," New Series, Vol. Ⅲ/27c1, Springer, Berlin (1997).

8 Y. Hinatsu, *J. Solid State Chem.*, **100**, 136 (1992).

9 Y. Hinatsu, *J. Solid State Chem.*, **102**, 362 (1993).

10 Y. Hinatsu and N. Edelstein, *J. Solid State Chem.*, **112**, 53 (1994).

11 Y. Hinatsu, M. Itoh, and N. Edelstein, *J. Solid State Chem.*, **132**, 337 (1997).

12 M. Itoh and Y. Hinatsu, *J. Alloys Comp.*, **264**, 119 (1998).

13 K. Tezuka, Y. Hinatsu, Y. Shimojo, and Y. Morii, *J. Phys.: Condens. Matter*, **10**, 11703 (1998).

14 M. Itoh, K. Tezuka, M. Wakeshima, and Y. Hinatsu, *J. Solid State Chem.*, **145**, 104 (1999).

15 K. Itoh, K. Tezuka, and Y. Hinatsu, *J. Solid State Chem.*, **157**, 173 (2001).

16 A. Callaghan, C. W. Moeller, and R. Ward, *Inorg. Chem.*, **5**, 1572 (1966).

17 Y. Maeno, H. Hashimoto, K. Yoshida, S. Nishizaki, T. Fujita, J. G. Bednorz, and F. Lichtenberg, *Nature*, **372**, 532 (1994).

18 A. W. Sleight and R. J. Bouchard, Solid State Chemistry, Proceedings of the 5th Materials Research Symposium, NBS Spec. Publ., **364**, 227 (1972).

19 N. Taira, M. Wakeshima, and Y. Hinatsu, *J. Solid State Chem.*, **144**, 216 (1999).

20 Y. Doi and Y. Hinatsu, *J. Phys.: Condens. Matter*, **13**, 4191 (2001).

21 N. Taira and Y. Hinatsu, *J. Solid State Chem.*, **150**, 31 (2000).

22 K. Henmi and Y. Hinatsu, *J. Solid State Chem.*, **148**, 353 (1999).

23 Y. Kanaiwa, M. Wakeshima, and Y. Hinatsu, *Mater. Res. Bull.*, **37**, 1825 (2002).

24 M. T. Anderson, K. B. Greenwood, G. A. Taylor, and K. R. Poeppelmeier, *Prog. Solid State Chem.*, **22**, 197 (1993).

25 Y. Doi and Y. Hinatsu, *J. Phys.: Condens. Matter*, **11**, 4813 (1999).

26 D. Harada, M. Wakeshima, and Y. Hinatsu, *J. Solid State Chem.*, **146**, 356 (1999).

27 M. Wakeshima, D. Harada, and Y. Hinatsu, *J. Mater. Chem.*, **10**, 419 (2000).

28 Y. Sasaki, Y. Doi, and Y. Hinatsu, *J. Mater. Chem.*, **12**, 2361 (2002).

29 K. R. Lea, M. J. M. Leask, and W. P. Wolf, *J. Phys. Chem. Solids*, **23**, 1381 (1962).

30 J. H. Van Vleck, "The Theory of Electric and Magnetic Susceptibilities," Oxford Univ. Press, Oxford (1931).

31 F. Grandjean and G. L. Long, "Mössbauer Spectroscopy Applied to Inorganic Chemistry," ed by G. J. Long, Plenum Press, New York (1984), Vol. 3.

32 J. M. Baker, *J. Phys. C*, **1**, 1670 (1968).

33 J. H. M. Thornley, *Proc. Phys. Soc. (London)*, **88**, 325 (1966).

34 P. D. Battle and W. J. Macklin, *J. Solid State Chem.*, **52**, 138 (1984).

35 R. Greatrex, N. N. Greenwood, M. Lal, and I. Fernandez, *J. Solid State Chem.*, **30**, 137 (1979).

36 P. D. Battle, C. W. Jones, and F. Studer, *J. Solid State Chem.*, **90**, 302 (1991).

37 P. D. Battle and W. Jones, *J. Solid State Chem.*, **78**, 108 (1989).

38 P. D. Battle, J. B. Goodenough, and R. Price, *J. Solid State Chem.*, **46**, 234 (1983).

39 T. Moriya, "Magnetism," Academic Press (1963), Vol. I, p. 85.
40 Y. Izumiyama, Y. Doi, M. Wakeshima, Y. Hinatsu, Y. Shimojo, and Y. Morii, *J. Phys.: Condens. Matter*, **13**, 1303 (2001).
41 Y. Izumiyama, Y. Doi, M. Wakeshima, Y. Hinatsu, K. Oikawa, Y. Shimojo, and Y. Morii, *J. Mater. Chem.*, **10**, 2364 (2000).
42 Y. Izumiyama, Y. Doi, M. Wakeshima, Y. Hinatsu, A. Nakamura, and Y. Ishii, *J. Solid State Chem.*, **169**, 125 (2002).
43 Y. Doi, Y. Hinatsu, A. Nakamura, Y. Ishii, and Y. Morii, *J. Mater. Chem.*, in press.
44 H. A. Blackstead, J. D. Dow, D. R. Harshman, D. B. Pulling, M. K. Wu, D. Y. Chen, and F. Z. Chien, *Solid State Comn.*, **118**, 355 (2001).
45 Y. Hinatsu, Y. Izumiyama, Y. Doi, M. Wakeshima, A. Nakamura, and Y. Morii, submitted.
46 D. Harada and Y. Hinatsu, *J. Solid State Chem.*, **158**, 245 (2001).
47 Y. Doi, Y. Hinatsu, K. Oikawa, Y. Shimojo, and Y. Morii, *J. Mater. Chem.*, **10**, 1731 (2000).
48 Y. Doi, Y. Hinatsu, K. Oikawa, Y. Shimojo, and Y. Morii, *J. Mater. Chem.*, **10**, 797 (2000).
49 R. D. Burbank and H. T. Evans, *Acta Crystallogr.*, **1**, 330 (1948).
50 J. Darriet, M. Drillon, G. Villeneuve, and P. Hagenmuller, *J. Solid State Chem.*, **19**, 213 (1976).
51 J. Darriet, J. L. Soubeyroux, and A. P. Murani, *J. Phys. Chem. Solids*, **44**, 269 (1983).
52 U. Treiber, S. Kemmler-Sack, A. Ehmann, H. U. Schaller, E. Dürrschmidt, I. Thumm, and H. Bader, *Z. Anorg. Allg. Chem.*, **481**, 143 (1981).
53 M. Rath and Hk. Müller-Buschbaum, *J. Alloys Compd.*, **210**, 119 (1994).
54 Hk. Müller-Buschbaum and B. Mertens, *Z. Naturforsch.*, **51b**, 79 (1996).
55 Y. Doi, M. Wakeshima, Y. Hinatsu, A. Tobo, K. Ohoyama, and Y. Yamaguchi, *J. Mater. Chem.*, **11**, 3135 (2001).
56 R. D. Shannon, *Acta Crystallogr., Sect. A*, **32**, 751 (1976).
57 H. Kobayashi, M. Nagata, R. Kanno, and Y. Kawamoto, *Mater. Res. Bull.*, **29**, 1271 (1994).
58 W. Bensch, H. W. Schmalle, and A. Reller, *Solid State Ionics*, **43**, 171 (1990).
59 C. W. Jones, P. D. Battle, and P. Lightfoot, *Acta Crystallogr., Sect. C*, **45**, 365 (1989).
60 P. C. Donohue, L. Katz, and R. Ward, *Inorg. Chem.*, **4**, 306 (1965).
61 P. Lightfoot and P. D. Battle, *J. Solid State Chem.*, **89**, 174 (1990).
62 D. Verdoes, H. W. Zandbergen, and D. J. W. IJdo, *Acta. Crystallogr., Sect. C*, **41**, 170 (1985).
63 Y. Doi, K. Matsuhira, and Y. Hinatsu, *J. Solid State Chem.*, **165**, 317 (2002).
64 J. T. Rijssenbeek, Q. Huang, R. W. Erwin, H. W. Zandbergen, and R. J. Cava, *J. Solid State Chem.*, **146**, 65 (1999).
65 I. Thumm, U. Treiber, and S. Kemmler-Sack, *Z. Anorg. Allg. Chem.*, **477**, 161 (1981).
66 Y. Doi, Y. Hinatsu, Y. Shimojo, and Y. Ishii, *J. Solid State Chem.*, **161**, 113 (2001).
67 Y. Doi and Y. Hinatsu, *J. Mater. Chem.*, **12**, 1792 (2002).
68 J. Willkens and Hk. Müller-Buschbaum, *Z. Anorg. Allg. Chem.*, **619**, 517 (1993).
69 H. W. Zandbergen and D. J. W. IJdo, *Acta. Crystallogr., Sect. C*, **40**, 919 (1984).
70 N. F. Mott and E. A. Davis, "Electronic Processes in Non-Crystalline Materials," 2nd ed, Clarendon Press, Oxford (1979).
71 J. T. Rijssenbeek, P. Matl, B. Batlogg, N. P. Ong, and R. J. Cava, *Phys. Rev. B*, **58**, 10315 (1998).
72 A. Abragam and B. Bleaney, "Electron Paramagnetic Resonance of Transition Ions," Oxford Univ. Press, London (1970), Chap. 5.
73 N. F. Ramsey, "Molecular Beams," Clarendon Press, Oxford (1956).
74 J. D. Axe, H. J. Stapleton, and C. D. Jeffries, *Phys. Rev.*, **121**, 1630 (1961).
75 S. Ohyama, Y. Doi, and Y. Hinatsu, unpublished results.
76 Y. Hinatsu, *J. Atomic Energy Soc. Japan*, **36**, 714 (1994).
77 Y. Doi and Y. Hinatsu, unpublished results.

Yukio Hinatsu was born in 1953 at Hikone in Shiga, Japan. He graduated from Osaka University in 1977 with a B.E. degree in nuclear engineering. He received his M.E. and D.E. degrees in nuclear engineering from Osaka University in 1979 and 1982, respectively. After graduation, he joined the Japan Atomic Energy Research Institute as a Research Scientist. He studied the chemical behavior of fission products from the nuclear spent fuel at the Oak Ridge National Laboratory in Tennessee, USA, as a visiting scientist for one and a half years in 1988-1989. Then, he moved to California and studied the electronic states of actinide ions in solids, at the Lawrence Berkeley Laboratory, University of California at Berkeley for a year in 1989-1990. Since 1995, he has been a full Professor of the Division of Chemistry, Graduate School of Science, Hokkaido University. His current research interests include the solid state chemistry and magnetochemistry of lanthanide and actinide compounds.

Yoshihiro Doi was born in 1975 in Hokkaido, Japan. He graduated with a B.Sc. degree from Hokkaido University in 1998. He also received his M.Sc. in 2000 and Ph.D. in 2002 from Hokkaido University, for his study of structural and magnetic properties of perovskite-related compounds. He was selected as a Research Fellow of the Japan Society for the Promotion of Science (JSPS) in 2000. Next, he has been appointed Research Associate of the Division of Chemistry, Graduate School of Science, Hokkaido University in 2002. His research interest is in the field of solid-state chemistry, and recently is focused on the perovskite-related compounds with novel magnetic properties due to the magnetic dimer and trimer.